# IMPLEMENTATION OF HIGH BANDWIDTH CONTROL FOR ROTARY AND LINEAR MOTOR DRIVES OF MILLING MACHINES

By

YAZID ELIAS TOHME

A DISSERTATION PRESENTED TO THE GRADUATE SCHOOL
OF THE UNIVERSITY OF FLORIDA IN FARTIAL FULFILLMENT
OF THE REQUIREMENTS FOR THE DEGREE OF
DOCTOR OF PHILOSOPHY

UNIVERSITY OF FLORIDA

2001

ACKNOWLEDGMENTS

I express my gratitude to Dr Jiri Tlusty for his guidance, support and patience over the past 5 years. I like to express my appreciation to Dr John Ziegert Dr John Schueller Dr Paul Mason, Dr Jacob Hammer and Dr Greg Sawyer for serving on my supervisory committee I also thank all of the members of the Machine Tool Research Center for their assistance and friendship I extend special thanks to Andrew Smith for his help in editing this manuscript.

TABLE OF CONTENTS

Abstract of Dissertation Presented to the Graduate School
of the University of Florida in Partial Fulfillment of the
Requirements for the Degree of Doctor of Philosophy

# IMPLEMENTATION OF HIGH BANDWIDTH CONTROL FOR ROTARY AND LINEAR MOTOR DRIVES OF MILLING MACHINES

By

Yazid Elias Tohme

December 2001

Chairman: Dr. John Ziegert
Major Department: Mechanical Engineering

This study compares ballscrew drives and linear motor drives for milling machine feed drives. In high-speed milling, feed drives with high accelerations are necessary to use the full capacity of the new high-speed spindles. Acceleration is limited by the lack of bandwidth in the position loop.

Two feed drives are investigated: a ballscrew drive and a linear motor drive. Descriptions of the mechanical and electrical components of each feed drive with emphasis on advantages and disadvantages is given. Proportional-derivative control schemes are implemented on each drive, and for the ballscrew drive a sliding mode controller is applied.

A ballscrew drive under PD control was found to have a 30 Hz bandwidth. This low bandwidth limits the maximum desired acceleration. The bandwidth was limited by structural resonances in the ballscrew. Use of digital filtering techniques increased the

bandwidth to 100 Hz, thus the ballscrew was able to reach a maximum acceleration of 2 g. The complexity in designing digital filters, their long calculation time and their lack of robustness make them undesirable in a machine tool controller. Therefore, a sliding mode controller was implemented as a substitute for the PD controller with digital filters to acquire a high bandwidth. This robust controller permitted a bandwidth of 65 Hz to achieve an acceleration of 1 g.

A linear motor drive under PD control was found to have a 70 Hz bandwidth. No additional filters were required to achieve this bandwidth. A major drawback of this drive is its sensitivity to changes of mass and to external disturbances like cutting forces and friction.

Feedforward filters were applied on both drives to decrease tracking errors during high acceleration moves. These feedforward filters reduced the tracking error to four counts on the ballscrew drive and to two counts on the linear motor drive.

# CHAPTER 1
# INTRODUCTION

High-speed machining evolved in the past decade as an improvement to conventional machining. Advancements in microprocessors and digital signal processors (DSPs) made it possible for the computer numerical control (CNC) to accurately control feed drives at high speeds. The processor evolution coupled with a high demand on delivering machined parts at lower cost and in faster times prompted the machine tool industry to produce machining centers dedicated only to high-speed machining. Furthermore, high-speed machining made it possible to replace other traditional manufacturing processes. For example high-speed machining of aluminum made it possible to produce monolithic parts to replace parts fabricated from several components. A machined part can be more accurate and structurally stiffer than a riveted part. From Zelinski [1] the speed brake of an F-15 fighter jet made by Boeing Aerospace, can now be machined from one piece of solid aluminum. Traditionally the 11 foot long, 3 foot wide part was made from sheet metal, a process that takes three months to assemble all the 500 components for one brake. The whole part can now be machined in 30 hours on a high-speed machine. The time and cost of the part is tremendously reduced, but more importantly, the quality of the part is improved.

Another example is the high speed machining of hard steel dies. High-speed machining of dies eliminates some of the steps from the traditional manufacturing process for dies. High speed machining makes it possible for the dies to be machined by taking

smaller tool steps thus improving surface finish and eliminating grinding and hand polishing

Several aspects make a machining center suitable for high speed machining maximum spindle speed, maximum feed drive speed lookahead and high data transmission rates Lookahead is a CNC feature that analyzes the commands beforehand to determine if the machine is capable of handling the commanded moves Smith [2] provided a more detailed description of high speed machine design

Although all of the above aspects are necessary for a high speed machine this work concentrates on the feed drive Specifically, the different types of feed drives that are suitable for these machines and the control methods that are implemented to make them perform coordinated moves at high speeds

Feed drives on high speed machining centers can exceed speeds of 0.5 m/s but that alone does not make them truly high speed High acceleration is required in order to attain the maximum velocity within the commanded move A high-speed feed drive must have high acceleration and high velocity

**High Speed Machining**

Most machined aircraft components like those in Figure 1-1 have small pockets to reduce their mass without diminishing their strength These pockets require that the feed drives of the machines reach the required speed as fast as possible in order to produce cost effective parts Feed drives on conventional machines can typically accelerate up to 0.3 g which is usually not sufficient for high speed machining of pockets Higher acceleration is required to take full advantage of the feed drives over short distances An example of the need for higher acceleration is the approximation of a helicopter rotor grip in

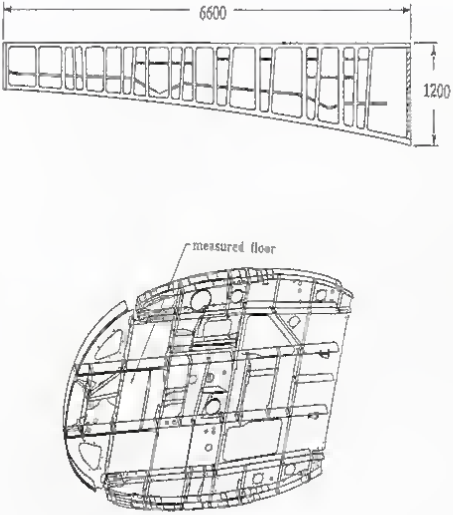


Figure 1.1 Example of thin aluminum parts

Figure 1 2. It was made from Al 7075-T6 and was machined using a conventional and a high-speed machine. The main pocket in the part was 63 mm by 114 mm. In Case *A* the conventional machine commanded a feedrate of 25 4 m/min at 0 2 g over the 114 mm travel. It took the drive 220 ms to accelerate to the commanded speed, then it traveled for 45 ms at constant speed before it started its deceleration. Most of the move was spent accelerating and decelerating the drive. In Case *B* the high speed machine was commanded the same position and velocity but a 2 g acceleration. The drive reached its maximum speed in 22 ms and traveled at the maximum speed for 247 ms before slowing. The total move was performed in 291 ms while it took 485 ms in case *A*. The entire part with its other features took 58 minutes to be machined on a conventional machine and took only 12 minutes to be high-speed machined. In the amount of time it took to produce one part on the conventional machine, five parts could be produced on the high speed machine.

In summary, it is important to increase the average velocity in order to reduce part production time. The goal is to achieve the highest acceleration possible.

**Acceleration and Bandwidth**

Acceleration is limited by two factors, thrust capacity of the drive and machine dynamics. Motors have limited peak accelerations defined by the maximum current that can be applied across the windings at a given time. In general, this is not the limiting factor. Acceleration is usually limited by machine dynamics. Vibrations in the drive prevent the machine from reaching high accelerations. The reason is that vibrations limit the overall positional bandwidth of the system. The bandwidth of the system is an indication of how the system responds to transients in the time domain.

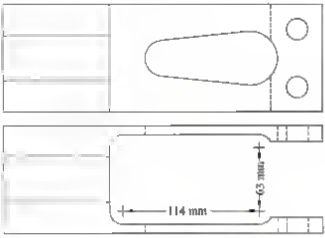


Case A
Feedrate 25 4 m/min
Acceleration 1 96 m/s$^2$ (0 2g)
Travel 0 114 m

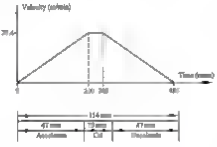


Travel 0 063 m

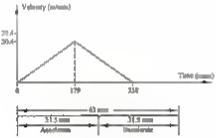


Case B
Feedrate 25 4 m/min
Acceleration 19 6 m/s$^2$ (2g)
Travel 0 114 m

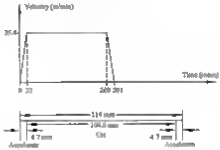


Travel 0.063 m

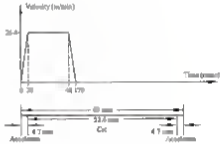


Figure 1 2 Bell helicopter rotor grip

Figure 1-3 shows how bandwidth and acceleration are related. From Case *A* and *B* in Figure 1-2, the desired accelerations look like impulse commands. The Fourier transforms of the impulses show the required bandwidths. The accelerations for machining the rotor grip require two different system bandwidth. Case *A* requires a very low bandwidth while Case *B* requires 10 times more bandwidths. It can be seen that high acceleration requires high bandwidth. The challenge in obtaining high bandwidth is the attenuation of structural modes within the desired bandwidth. Conventional ballscrew drives generally have modes less than 100 Hz. These modes require low-pass filtering to reduce their effects. These low-pass filters limit the overall bandwidth.

Two approaches can be taken to improve bandwidth: the first is to re-design the drive to have all modes above 100 Hz or to use a different control method that attenuates the modes in the control loop. The first approach is the most widely accepted in industry. Conventionally designed drives with rotary motors and leadscrews are being replaced with linear motors. Because linear motors usually have modes at higher frequencies they are suitable substitutes for ballscrews in some cases. They have limiting factors that are different than ballscrew drives and cannot be switched without proper analysis. The second approach is to modify the control system. Control methods can attenuate or reject modes and increase the overall bandwidth. The difficulty is in implementing these control schemes. Off the shelf controllers are programmed for PID control which is a simple linear control theory that is widely understood and used...but this theory is not capable of dealing with structural modes within the bandwidth. A more elaborate control method is required.

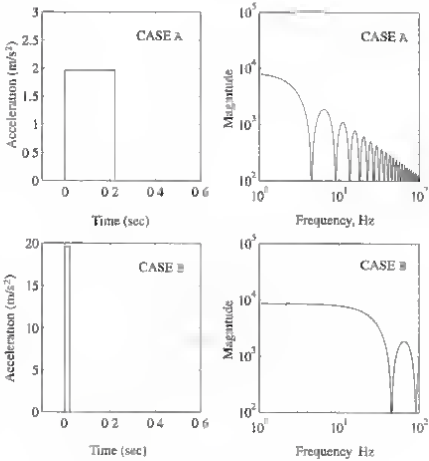


Figure 1-3 Acceleration and bandwidth

Finally moving feed drives at high speeds develops large tracking errors Tracking errors are the difference between the commanded and actual positions, as shown in Figure 1-4 These errors can cause imperfections in the machined parts especially when there are multiple axes moving simultaneously Again control theory can reduce these errors and improve part quality

**Test Beds**

The Machine Tool Research Center (MTRC) at the University of Florida has designed two high-speed milling machines to be used as test beds for the development of high speed machining Figure 1-5 shows the UF MTRC HSM1 which is a horizontal five-axis high speed milling machine, and Figure 1-6 shows the UF MTRC HSM2 vertical three-axis high-speed milling machine Both of these machines are equipped with open architecture control systems that permit the implementation of user-written servo algorithms The HSM1 serves as the test bed for this study The Y-axis consists of a ballscrew and a rotary motor This drive is tuned with a PID controller with digital filters and is also re-tuned for a sliding mode controller The Z-axis of the machine is driven by two linear motors and is tuned with a simple PID Both axes are used to compare and contrast ballscrew drives and linear motor drives

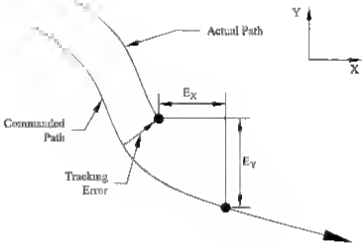


Figure 1-4 Tracking error

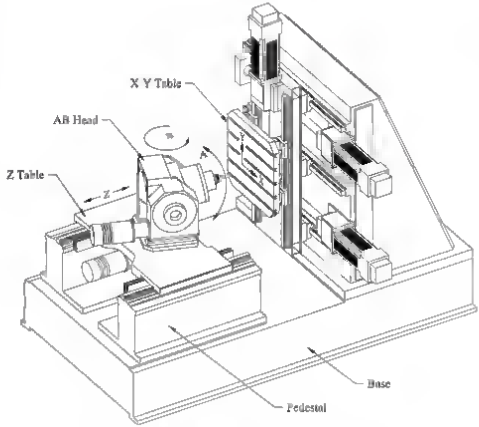


Figure 1-5 High speed milling machine (HSM1) at UF_MTRC

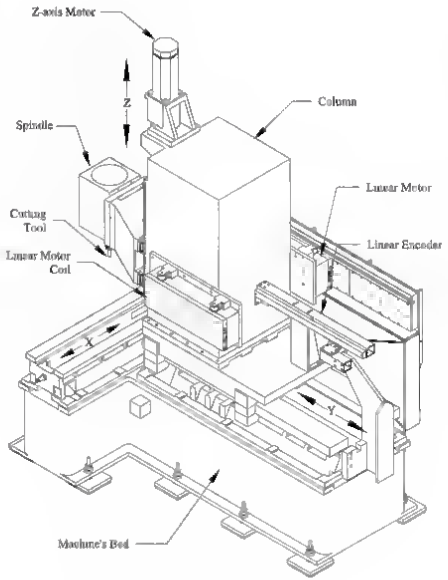


Figure 1-6 High speed milling machine (HSM2) at UF_MTRC

# CHAPTER 2
# LITERATURE REVIEW

Computer Numerical Control (CNC) has become the most important part of modern machine tools. With the continued development of microprocessors, CNC machines have become more technologically advanced in their computing power. Today's machine tool controllers may possess several processors, some for generating commands and others for applying control algorithms on the drives. Some controllers even have dedicated processors for every drive on the machine. Machine tools have entered the digital world, and with this new technology, advanced control strategies can be more easily implemented and evaluated.

In order to test control strategies, an acceptable controller must be found. Conventional CNC technology is built around proprietary architectures with incompatible software and operating protocols. Additionally, these controllers are expensive and costs to enhance their flexibility are prohibitively high. Open architecture controllers generally allow researchers to implement and evaluate more complex control strategies on machines in less time and at a lower cost than previously possible. With the flexibility of the open architecture controller, machine tool research has become more focused on speed and precision.

This chapter reviews some of the work other researchers have conducted in the control of machine tool drives.

## Control Theory

In general two types of control strategies applied to machine tools–open loop control used with stepper motors and closed loop (feedback) control used with servomotors. Only closed loop control can provide the degree of tracking accuracy necessary for high-speed, high-precision metal cutting. A closed loop feedback controller compares the actual output from the drive to the desired input, determines the error and produces a control signal to eliminate it. [3] The most widely used controller theory is the Proportional-Integral-Derivative (PID) controller.

### PID Controller

The basic PID controller in Figure 2-1 compares the positional feedback to the desired position, computes the error, and tries to eliminate it. This controller uses proportional, integral, and derivative gains to adjust the performance of the system. The advantages of this controller include that it is simple to install and it is easily understood by most engineers.

The principal disadvantage of a PID controller is that it cannot deal with nonlinearities. Nonlinearities which arise from friction, cutting forces, and machine structural modes cannot be easily compensated by a PID controller. These nonlinearities may cause instability which limits the closed loop position bandwidth of the system, and results in low performance.

### Feedforward Techniques

Some researchers have modified the basic PID controller to compensate for some of the nonlinearities by adding feedforward terms to the control loop. Tlusty and Chen [4]

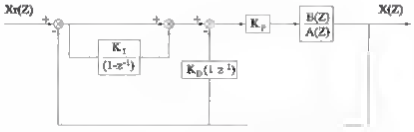


Where: $K_P$ = is the Proportional Gain. $K_I$ = is the Integral Gain.
$K_D$ = is the Derivative Gain
$\frac{B(Z)}{A(Z)}$ = is the Open Loop Transfer Function.

Figure 2-1 Proportional-Integral-Derivative Controller

dealt with the cancellation of vibrations of lowly damped structural modes that limit bandwidth. They suggested three different alternatives to eliminate the lowly damped structural modes. The first alternative used a feedforward compensation filter that cancelled out the lowly damped mode and was implemented using a rotary encoder. The second alternative used a linear encoder, a similar feedforward compensation filter, and accelerometric feedback to increase system performance. The third alternative used a tuned passive damper to modify the dynamics of the servodrive. The disadvantage of the first and third alternatives is that they cannot compensate for frequencies of the lowly damped modes that change with the motion of the machine. In other words, the feedforward compensation filters are tuned to cancel only one specific frequency.

Weck [5] introduced an inverted system model (IKF) and a low pass filter to compensate for undesired frequencies. The IKF controller can increase the tracking performance of the drive, but it is only useful for linear systems. Furthermore, like the Tlusty and Chen model, it cannot readily compensate for any nonlinear structural modes.

**Zero Phase Controller**

Tomizuka [6] introduced the zero phase error tracking controller (ZPETC) to improve performance. This feedforward controller cancels all closed loop poles and all closed loop zeros that are inside the unit circle. It also cancels all phase shifts of the closed loop zeros that are outside the unit circle. The result is a frequency response that exhibits zero phase shift between the desired and actual output at all frequencies. Since this controller could not be easily implemented on an actual servodrive, Tomizuka and Yao [7] developed an adaptive version of the ZPETC that uses a pole placement controller algorithm.

**Pole Placement Control**

Altintas and Erkorkmaz [8] applied a pole placemant controller showo in Figure 2-2 with Kalman filters and friction compensation. The values of the polynomials $R(z)$, $S(z)$ and $T(z)$ were determined by comparing the closed loop transfer function in Equation 2-1 to a desired model $B_m(z)/A_m(z)$. The system $B(z)/A(z)$ was identified using white noise excitation and a least squares method.

$$\frac{X(z)}{X_r(z)} = \frac{A_0 \quad BT}{A_0 AR + BS} \tag{2-1}$$

Kalman filters are used to reject noise and disturbances. The main limitation of this type of controller is that it cannot cope with any changes in the system $B(z)/A(z)$. For example if the system is not precisely identified or is nonlinear then the overall system may become unstable.

**H-Infinity Control**

Van Brussel [9] implemented an H infinity algorithm to control linear motors with a varying table mass as a parametric uncertainty. He found out that the tracking error becomes too high when the mass is increased to 300%. He also concludes that the limitations of the control method are due to poor selection of weighting functions.

**Sliding Mode Control**

Sliding mode control theory (SMC) is becoming a favorite for machine tool researchers. It is a variable structure controller that does not require precise system identification. Slotine [10] describes the methodology for implementing a sliding mode controller and for correcting problems like chatter.

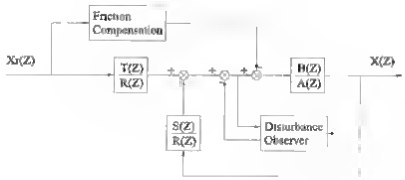


where

$A(z)$ = The poles of the system

$B(z)$ = The zeros of the system

$R(z)$ = Polynomial , where the degree of $R$ = deg $(A_0 + A_m \ A)$

$S(z)$ = Polynomial where the degree of S< deg R

$T(z)$ = Polynomial where the degree of $T$ = deg $(A_0 + B_m)$

$A_0(z)$ = Polynomial where the degree of $A_0$ = 2 deg $A(z)$ deg $A_m(z)$ - 1

Figure 2 2 Pole Placement Controller

Van Brussel [9] implemented an SMC and found that the tracking error remains at 6 $\mu$m, even if the moving mass on a linear motor was increased by 300% but did not discuss the overall bandwidth of the system. Altintas and Erkorkmaz [8] used the SMC to control rotary servomotors and were able to achieve a positional bandwidth of 100 Hz.

**Other Control Theories**

Boucher [11] used a generalized predictive cascade control (GPCC) algorithm. By predicting the behavior of the plant for a defined bandwidth, he generated a set of future control values to minimize the error. Koren and Lo [12] used a variable-gain cross coupling controller that generated correction signals for each axis based on contouring errors supplied through feedback from all axes on the machine.

**Linear Motors**

Some of the conventional drives on high speed milling machines are being substituted by direct drives that use linear motors. Pritschow [13] discussed the advantages of linear motors over conventional drives in high-speed machining as well as the differences among the different types of linear motors. He concluded that because of the absence of compliant transmission elements, linear motors can have larger position loop bandwidths and higher accelerations than conventional rotary servomotors. Furthermore, linear motors can deliver higher speeds which increase the productivity of the machine. Finally, he notes that DC linear motors are more suitable in machine tool applications than AC induction type linear motors because of their ability to deliver a higher force per unit weight of the magnets and coils.

# CHAPTER 3
# DESIGN FOR LINEAR MOTION

Linear motion in high performance milling machines centers on using two basic axis drive designs: the leadscrew drive and the linear motor drive. The leadscrew drive offers a low-cost drive with high stiffness; and because of the transmission ratio, it is insensitive to changes in workpiece mass. The linear motor drive offers higher speeds and higher accelerations, but since it is a direct drive, it is very sensitive to changes in workpiece mass and to external disturbances. In this chapter, both drives are discussed to evaluate their strengths and weaknesses.

## Leadscrew Drives

A leadscrew drive is the most commonly used actuator for high performance axis drives in milling machines. The drive in Figure 3-1 shows a leadscrew drive. The leadscrew is coupled to a rotary servomotor that rotates the leadscrew in the bearings. The table and nut are driven down the helical thread of the leadscrew.

### Components of Leadscrew Drives

Direct-current rotary servomotors are the most widely used type of motors in milling machines. Direct-current servomotors are better suited for machine tool applications than AC motors because they have a lower moment of inertia and can provide higher peak accelerations than AC servomotors.

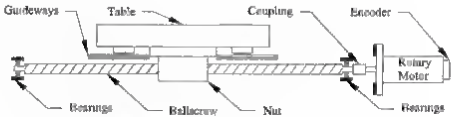

Figure 3-4 Conventional ballscrew drive

The servomotor is connected to the leadscrew using a flexible disk coupling that allows for small angular and axial misalignment between the motor shaft and leadscrew end yet provides high torsional rigidity Unfortunately to obtain the high torsional stiffness, a large coupling is used which has a high moment of inertia.

The leadscrew is held in two sets of end bearings The bearings – typically a pair of angular contact ball bearings or tapered roller bearings – closest to the motor handle all of the axial loads imposed on the leadscrew The "free end of the leadscrew is held by a radial bearing The radial bearing allows for thermal expansion of the leadscrew and raises the minimum critical speed of the leadscrew

Conventionally the ballscrew is the preferred leadscrew in high-speed drives. Precision ballscrews have three components a screw, a nut and recirculating balls The balls recirculate through concave helical grooves ground in both the screw and the nut Backlash is eliminated by squeezing the balls between the screw and the nut. This is achieved by having a nut with two halves which have slightly mismatched grooves The ballscrew is limited in speed and acceleration because of the recirculating balls

An alternative to the ballscrew is the hydrostatic leadscrew High pressure oil is supplied to pockets that are machined in the threads of the nut This oil suspends the nut from the screw which makes the hydrostatic drive non contact and nearly frictionless The speed of the hydrostatic leadscrew is limited by hydrostatic fluid cavitation or pocket starvation

**Advantages and Disadvantages of Leadscrew Drives**

The first disadvantage is the limited life of a ballscrew due to wear caused by mechanical contact. This is not a problem for the hydrostatic leadscrew

The second disadvantage is limited speed and travel based on the screw diameter and length. A ballscrew is limited by critical speed or ball speed. A longer leadscrew of fixed diameter has a lower critical speed depending on end bearing arrangement. A larger diameter screw has a lower maximum operating speed because of the higher peripheral velocity of the balls.

A third disadvantage is the limited position bandwidth that can be achieved with a leadscrew. Leadscrews can have torsional vibrations which limit the bandwidth. Low pass filters are commonly used in machine tool drives to attenuate higher frequencies and stabilize the control loop. However, low pass filters were not used by Tlusty [14] and Smith [15] because they decrease the performance of the drive by decreasing the overall bandwidth of the system. The peaks were eliminated by inserting an inverse filter in the feedback loop that canceled both resonances. These digital filters extended the position loop bandwidth up to 100 Hz. The problem with such a design is that a change in the drive dynamics can allow a mismatch between the filters and the open loop response thus causing an unstable system. Also an additional controller was required to handle the calculations of the filters for every servo loop.

A fourth disadvantage is the location of the feedback devices. From Figure 3-1 rotary encoders are typically mounted on the back end of rotary motors to provide position feedback. The rotary encoders may not sense the actual position of the table due to mechanical vibrations outside the control loop or thermal expansion. This can lead to inaccuracies in the machined part. An alternative is mounting linear encoders parallel to the motion of the table that can report accurate table positions. The linear encoder senses

vibrations which were previously outside the position loop These vibrations may destabilize the position loop if uncompensated.

A disadvantage of a hydrostatic screw is that it requires a continuous supply of cool, high pressure oil This requires a supply pump an oil reservoir, a heat exchanger and a chiller Additionally, the hydrostatic oil must be captured upon leaving the nut and must be isolated from other fluids

Advantages of a leadscrew drive includes low cost simple assembly procedures low sensitivity to changes in workpiece mass and high static and dynamic stiffiness

**Linear Motor Drives**

A linear motor drive is a direct drive which acts directly on the table mass without a transmission Linear motors are mounted parallel to the guideways with the shorter motor assembly attached to the table and the longer assembly attached to the bed An optical linear encoder is mounted parallel to the motion and provides position feedback The direct drive eliminates all mechanical transmissions therefore all the performance of the drive is limited to one component – the linear motor

Fundamentally linear motors are rotary motors rolled out flat as shown in Figure 3-2 The moving part is typically called the rotor and the fixed part the stator Linear motors are divided into two main groups AC motors and DC motors AC motors are also divided into two subcategories the linear inductance motor and the linear reluctance motor Generally AC motors are used for movement over long distances as in rail locomotives while DC motors are used for precise movement over shorter distances DC motors are divided into three subcategories the moving magnet the iron core and the ironless motors

**Components of DC Linear Motor Drives**

The two primary components of brushless DC linear motors are the permanent magnet assembly and the coil assembly. The basic theory behind the operation of linear motors is similar to that of rotary motors. When the conductors of a certain length $l$ in the coil carries a current $I$ in a direction perpendicular to the magnetic field of flux density $B$ the coil experiences a force $F$ perpendicular to both the direction of the current flow and the magnetic field. Figure 3-3 shows the orientation of $I$, $B$ and $F$. The magnetic field is generated by permanent magnets. The magnets used on the linear motors at UF MTRC high-speed milling machine are a neodymium iron-boron ceramic magnets which produces a stronger field than standard magnets.

From Basak [16] the brushless DC linear motors are divided into three categories moving magnet motors, moving armature motors (or iron core motors) and moving coil motors (or ironless motors).

A moving magnet motor is similar to the brushless rotary motor. Figure 3-4a shows how the stator is made from laminations while the rotor is made from permanent magnets. These motors have a high power loss making them very inefficient compared to the moving armature motor.

The moving armature motor of Figure 3-4b has stationary magnets and moving laminations. They are more efficient than the moving magnet motors because the windings are opposed by magnets at all time.

The third type is the moving coil motor of Figure 3-4c. It is similar to the moving armature magnet except the laminations are free of iron which eliminates cogging force.

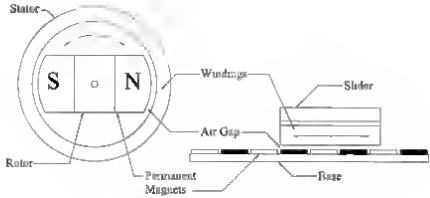


Figure 3-2. Rotary motor rolled out flat

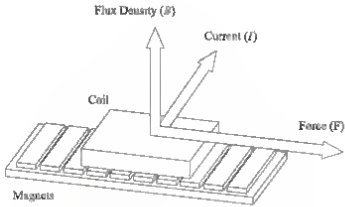


Figure 3-3 Magnet and coil assembly

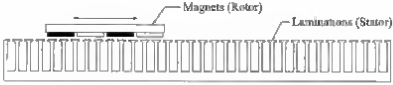


a) Moving Magnet Motor

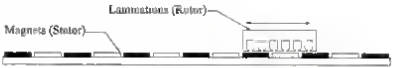


b) Moving Armature Motor

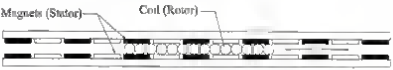


c) Moving Coil Motor

Figure 3-4 The three different types of DC linear motors

Magnets on both sides of the motor are used to generate more thrust force and provide a flux return path for the magnetic circuit

For this work the motor that best fits the application and constraints is the iron core motor Table 3-1 shows some of the differences between the three motors Although the characteristics of the ironless motor are desirable, the thrust force of the available sizes is too weak for the application Because of the inefficiency of the moving magnet motor, the iron core motor is the best suited motor

Table 3 1 Comparison of brushless direct-current linear motors

| | Moving magnet | Iron core | Ironless |
|---|---|---|---|
| Weight of moving unit | Medium | High | Light |
| Cost | Moderate | Low | High |
| Cogging force | Present | Present | None |
| Thrust force capabilities | High | High | Low |
| Efficiency | Low | Medium | High |

**Advantages and Disadvantages of Linear Motor Drives**

One disadvantage of large linear motors is heat generation The coils are very large in size and need to be cooled in order to achieve the highest efficiency The required cooling system increases the cost and complexity of the machine Also temperature sensors are needed to monitor the motor continuously

The second disadvantage is that linear motors have low efficiencies This low efficiency is mainly due to large air gaps between the stator and the rotor This gap allows a high flux leakage From Basak [16] the efficiency of some linear motor could be less than 50%

A third disadvantage is the high lateral attractive force. The iron core motors unlike the ironless motors have a large attraction between the magnet and the steel laminations in the coil. These forces can be as much as three times larger than the thrust force. The attractive force of the motors selected for this work is about 35 000 N while the thrust force is only 13 000 N. This attractive force can exert a large force onto the guideways increasing friction and wear in the guideways. It is possible to cancel this attractive force by mounting two linear motors back to back. This large force also causes problems during installation. Mounting procedures must prevent the coils and the magnets from touching. If the coil gets stuck on the magnets, removal may be impossible without damaging the motor.

The fourth disadvantage is that linear motors must be protected from chips that are attracted to the magnetic components. Metal chips can be pulled into the air gap leading to a short and damaging the coils.

The fifth disadvantage in linear motors is that the table cannot be held in position without power. There is nothing to stop the motion of the mass in case of a loss in power. Additionally, an external brake is required for vertical applications.

The sixth disadvantage is cogging forces in the iron core motor. These cogging forces are about 5% of its continuous force. These disturbances cause unacceptable position error and must be compensated.

The seventh disadvantage is the high sensitivity to changes in workpiece mass or external force disturbances like cutting forces and friction forces. Figure 3-5 shows the step response of a linear motor for two different masses without retuning the servo loop.

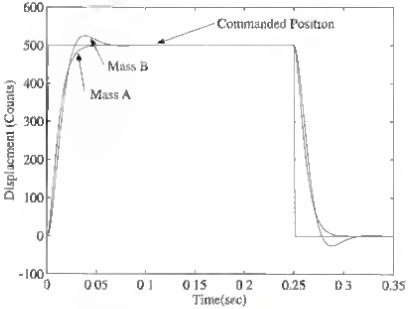


Figure 3 5 Step response with two different masses

The mass in case *B* is twice the mass in case *A*. Similarly, external forces will cause position changes.

The main advantage of direct drives is the speed and acceleration they can provide. Linear motors can achieve speeds up to 250 m/min, about 5 times more than leadscrew drives. They can achieve high accelerations, up to 10 g unloaded. High bandwidth is easily achievable with minimal control work.

Another major advantage is the stiffness. Overall stiffness is highly desirable in machine tools. Reportedly, linear motors can have higher stiffnesses than leadscrew drives [13]. Stiffness in linear motors is dependent on the position loop tuning. High gains in the position loop can increase stiffness in the drive.

**Summary**

A comparison between a linear drive and a leadscrew drive is shown in Table 3-2. In summary, the linear motor drive can achieve a higher acceleration than a ballscrew drive, its major drawback is its sensitivity to mass changes and external disturbances.

Table 3-2. Comparison between linear motor drive and leadscrew drive

| | Linear motor drive | Leadscrew drive using a brushless rotary motor |
|---|---|---|
| Speed | High speeds up to 250 m/min | Limited to the leadscrew s maximum speed |
| Acceleration | High (Limited by the motor peak acceleration) | Limited by flexibilities of the screw |
| Travel | Unlimited travel | Limited travels |
| Sensitivity to mass changes | High | Low |
| Sensitivity to external loads | High | Low |
| Cogging force | High (about 5% continuous force) | Moderate (about 1% continuous force) |
| Backlash | None | Some |
| Dynamic stiffness | High (Depending on tuning) | High |
| Installation | Complicated | Simple |
| Operating life | High (No wear) | Limited life |
| Efficiency | Low | High |
| Cost | High | Low |

# CHAPTER 4
# TUNING ROTARY MOTOR DRIVES FOR WIDE BANDWIDTH

The geometry of most aircraft parts includes deep pockets with small dimensions. High-speed machining these pockets requires high accelerations in order that the maximum speed can be reached over the short distance. A common aircraft part requires more than 500 acceleration and deceleration commands in less than one minute. Only a feed drive with wide enough bandwidth can accurately track such commands. Wide bandwidth is not easily achievable because structural modes in the drive limit bandwidth.

As mentioned earlier, there are two methods to achieve a high bandwidth feed drive: altering or improving the control method to deal with these structural modes, and redesigning the feed drive axis using linear motors. The next chapter deals with the control of a linear motor, while this chapter investigates the source of the structural modes and methods to treat them in the control system.

The high speed milling machine HSM1 at the MTRC is used as a test bed to show the differences between the two different drives. The machine's Y-axis illustrates the use of a traditional ballscrew drive. The feed drive consists of both electrical and mechanical systems which include: the controller, PWM amplifier and power supply, the servomotor, encoder, tachometer, ballscrew, ballnut, bearings, and the moving mass.

## Analysis of Leadscrew Feed Drives

The ballscrew drive is shown in Figure 4-1. The ballscrew is driven by a permanent magnet brushless DC servomotor made by Kollmorgen, model number B-804B. The servomotor has permanent neodymium iron boron alloy magnets attached to the rotary shaft and a six-pole three-phase Y-stator windings attached inside a cast aluminum housing. A resolver, a tachometer, and an encoder are mounted at one end of the motor shaft, and on the opposite side the ballscrew is coupled through a flexible coupling. The motor is driven by a PWM (Pulse Width Modulation) amplifier which is set to operate in the current mode. The resolver is fed back into the amplifier and is used to provide a commutation signal. The velocity loop is closed with a 17 V/krpm tachometer and the position loop is closed through an A-B quadrature encoder with 20 000 counts per revolution. Both the velocity and position loops are closed in the controller. The flexible coupling is attached to a ballscrew that is 52 inches long. The ballscrew is attached to the driven load or table through a ballnut. The lead of the ballscrew is 20 mm per revolution.

The controller uses from two separate components. The first component is the commercial CNC controller PMAC by Delta Tau. This controller is used for data acquisition, command generation, and other CNC housekeeping functions like executing PLC's and event monitoring. This controller uses the Motorola 56300 fixed point DSP chip, which is not capable of handling the time processing of high order digital filters. The second controller is a commercial floating point DSP board which is used only for the control loops. This DSP board allows the implementation of any control strategy as long as its computation time for all the axes does not exceed the servoloop closing time. The servoloop time is set at 221 μs.

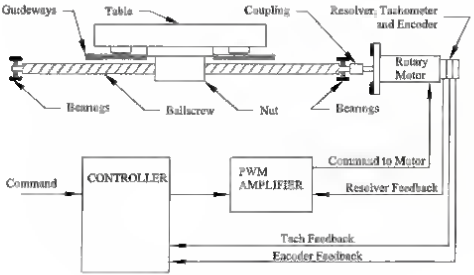


Figure 4–1 Rotary motor and ballscrew drive

**Leadscrew Drive Model**

The block diagram shown in Figure 4-2 represents the model of the uncoupled rotary motor powered by the PWM amplifier. In order to properly analyze the system some simplifications have been made to reduce the order and the complexity of the system. The electrical part of the motor is neglected since its time constant is faster than that of the mechanical system. The back emf and the current loop are omitted because they both have high bandwidth and little dynamics that could affect the position loop bandwidth of the system. The motor's viscous friction coefficient $B$ is neglected since it is negligible in size. Figure 4-3 shows the simplified block diagram with the low pass filters in the amplifier and the tachometer. The low pass filter on the tachometer is set at 2,000 Hz and is used to reject high frequency noise such as PWM from the amplifier and to prevent aliasing after the analog signal is converted to a digital signal. The open loop transfer function between the input signal to the amplifier and the output signal from the tachometer can be represented by the following equation

$$G_{vp}(s) = K_a K_T H_T \times \frac{\omega_{ca}^{\ 2}}{(s+\omega_{ca})^2} \times \frac{\omega_{cl}}{(s+\omega_{cl})} \times \frac{1}{Js} \qquad (4\text{-}1)$$

This continuous time open loop transfer function $G_{vp}(s)$ is converted to a discrete time $G_{vp}(z)$ using a zero order hold to accurately describe the system and is given in Equation 4-2. The discrete system equation can now be used to compare the systems actual behavior with the simulated behavior.

$$G_{vp}(z) = \left(\frac{z-1}{z}\right) Z\left\{ L^{-1}\left[ K_a K_T H_T \left(\frac{\omega_{ca}^{\ 2}}{s+\omega_{ca}^{\ 2}}\right)\left(\frac{\omega_{cl}}{s+\omega_{cl}}\right)\frac{1}{Js^2}\right]\Bigg|_{t=kT}\right\} \qquad (4\text{-}2)$$

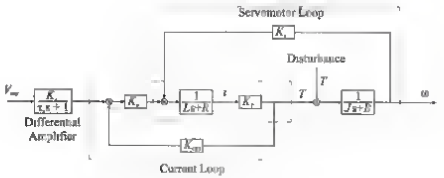


Figure 4-2 Block diagram of the open-loop

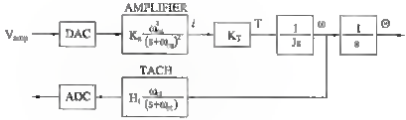


Figure 4-3 Block Diagram of transfer function

Table 4-1 shows the values of constants in Figure 4-3 and Equation 4-2 as supplied by the manufacturers

Table 4-1 Values for ballscrew drive parameters

| | |
|---|---|
| Amplifier cutoff frequency | $\omega_{ca} = 6300$ rad/s |
| Tachometer low pass filter frequency | $\omega_{ct} = 12600$ rad/s |
| Amplifier gain | $K_a = 15.1$ A/V |
| Torque | $K_T = 1.646$ Nm/A |
| Tachometer sensitivity gain | $H_T = 0.0477$ V/(rad/s) |
| Rotor moment of inertia | $J = 0.00840$ kg m$^2$ |

The transfer function of the actual system is then obtained by performing a sine sweep test on the feed drive A sine sweep test is a method used to determine the transfer function of a system A series of sine waves with equal amplitudes and varying frequencies are generated stored on the controller and then sent to the servomotor via the amplifier in an ascending order As the wave causes the motor to oscillate the feedback sensors are sampled by the controller In this case the feedback sensors are the tachometer and the encoder After all the data is collected a Fourier transform is applied to the sampled tachometer response and the result of the output over the input is the transfer function

The result of the sine sweep test is the transfer function plot in Figure 4-4 The figures of the transfer functions show two separate plots: the magnitude and the phase The bandwidth of a system is defined as the frequency range before the magnitude drops below -3db The phase plot shows the phase shift at each frequency The system in Figure 4-4 has a slope because this is the result as seen from the tachometer which measures velocity The encoder is also sampled but because the tachometer is more

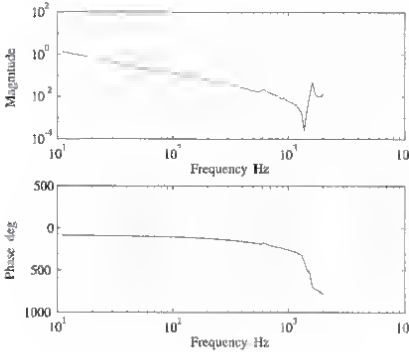


Figure 4-4 Open loop TF without Ballscrew

sensitive. It is used to generate the transfer functions. Integration of the tachometer signal yields the position signal. The figure shows that there are no noticeable vibrations under 1 000 Hz, the cutoff frequency of the amplifier. This means that up to the cutoff frequency the relationship between the command and the actual velocity is one to one. A 3 000 rpm command yields a 3 000 rpm response. At frequencies higher than the cutoff frequency the relationship between the command and actual velocity is attenuated. The phase plot represents the time shift or a time delay between the command and actual velocity.

After the sine sweep test is completed, the ballscrew is coupled to the motor. A second sine sweep test is executed and Figure 4-5 shows the open loop transfer function of the system with the ballscrew. As expected, several dynamics associated with the coupled load appeared. These plots show modes at 50, 550 and 1 050 Hz. These modes cause instability in the control loop if a 100 Hz bandwidth is to be achieved. Removal of them requires identifying their sources.

**Leadscrew Modal Identification**

In order to understand the behavior of the system, a more thorough understanding of the system is required which leads to the development of a more accurate transfer function model. The modes in Figure 4-5 are from torsional and axial flexibilities associated with the table, ballnut, ballscrew, coupling, and motor assembly. These lowly damped, second-order vibrations can cause the system to become unstable when they are introduced in to the closed position loop. In most conventional machine tool applications low-pass filters are inserted into the position loop to attenuate these vibrations, but they also limit the system's bandwidth. The objective in this work is to design digital filters that remove these vibrations and still keep a wide bandwidth up to 100 Hz. First a model

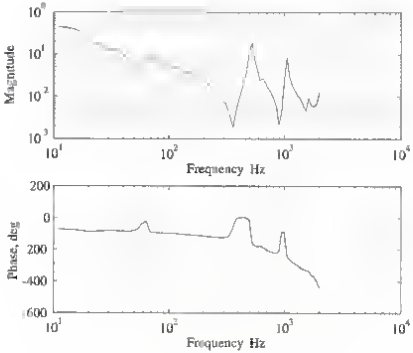


Figure 4-5 Open loop with ballscrew

of these second order dynamics must be added to the discrete transfer function in Equation 4-2. Figure 4-6 shows the free body diagram of a second order system model. From Newton s second law of motion Equation 4-3 is obtained

$$m\ddot{X} + c(\dot{X} - \dot{X}_r) + k(X - X_r) = 0 \tag{4-3}$$

A Laplace transform to Equation 4-3 yields the following

$$\frac{X(s)}{X_r(s)} = \frac{cs + k}{ms^2 + cs + k} \tag{4-4}$$

where

$m$ = The mass of the column (kg)
$c$ = Damping coefficient (N/(m/s))
$k$ = Spring stiffness (N/m)

Each of the three modes is modeled as a second order system as shown in Equation 4-4. They are then cascaded together to form the entire transfer function. These vibrations are then classified into two types: inside the loop and outside the loop. Vibrations inside the loop cause system instability; these have to be removed in order to achieve wide bandwidth. Vibrations outside the loop do not cause stability problems, but they might leave undesirable machining marks on the parts. Figure 4-7 shows the system $G_p(s)$ with two second order modes that are added to the inertia of the system and are considered inside the loop. The variables in Figure 4-7 are derived from the variables from Equation 4-4. Equation 4-5 shows the relationship. The values of these variables are computed from measurements conducted on the actual system and from data supplied by manufacturers. The value of the total system moment of inertia is calculated by summing all of the inertia of the moving parts in the system.

$$\omega_n = \sqrt{\frac{k}{m}} \qquad \zeta = \frac{c}{2\sqrt{k \times m}} \tag{4 5}$$

where

$\omega_n$ = Natural frequency (rad/s)

$\zeta$ = Damping ratio (N/m)

This includes the moments of inertia of the following the rotor or motor shaft coupling ballscrew ballnut and table The table and ballnut inertia are calculated as reflected on the motor shaft Table 4-2 shows the moments of inertia of all the components of the Y axis on HSM1

Table 4-2 Moments of inertia of the ballscrew drive

| Description | Moment of inertia J (Kg m$^2$) | Perceotage |
|---|---|---|
| Ballscrew | 0 00182 | 56 6 |
| Rotor | 0 00840 | 26 |
| Table and nut | 0 00820 | 2 5 |
| Coupling | 0 00485 | 15 |
| Total | 0 03227 | 100 |

Figure 4-8 shows the open loop model with $G_f(s)$ that includes two structural modes added to it. The remaining values are then extracted from actual measurements

Two of the modes that are inside the loop are suspected to be torsional flexibilities in the ballscrew and motor assembly A test is performed to properly identify them Two accelerometers mounted opposite each other are used to sense torsional vibrations and reject axial vibrations The same sine sweep test used for the previous open loop measurements is conducted again The result is shown in Figure 4-9 which shows the mode shapes of the ballscrew at the 550 and 1,150 Hz modes This test proves that two

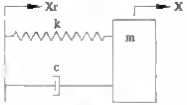


Figure 4-6 Spring Mass Damper model

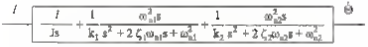


Figure 4-7 Dynamics

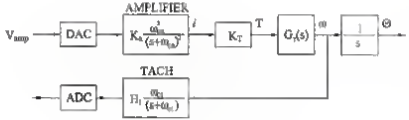


Figure 4-8 Open loop with dynamics

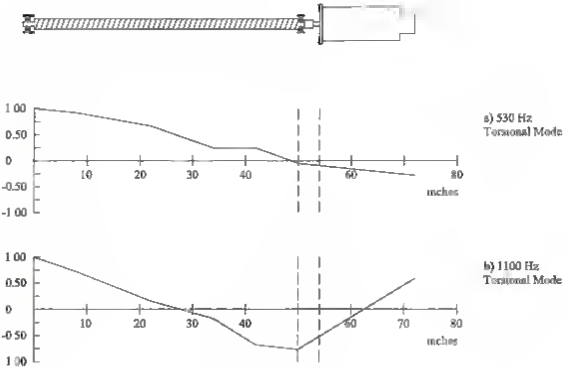


Figure 4-9 Ballscrew mode shapes

modes are indeed inside the loop and are associated with the torsional flexibilities of the system

A impact test measurement on the moving mass of the Y table using an instrumented impact hammer and an accelerometer confirms that the 50 Hz mode is an axial flexibility in the table along its direction of motion These values are then used to generate an accurate model of the overall system

The new model of the system is obtained by combining the open loop transfer function represented by Equation 4 2 with the system shown in Figure 4-7

$$G_{vb}(z) = \left(\frac{z-1}{z}\right) Z\left\{ L^{-1}\left[ K_v K_T H_T \left(\frac{\omega_{cu}^2}{s^2+\omega_{cu}^2}\right)\left(\frac{\omega_{ca}}{s+\omega_{ca}}\right)\frac{G_r(s)}{s}\right]_{t=KT}\right\} \qquad (4\ 6)$$

Using Equation 4-6 and the transfer function measurement from Figure 4 5 the values for the flexibilities are approximated by best fitting the model to the actual transfer function Figure 4-10 shows both the actual transfer function represented by the solid line and the modeled transfer function represented by the dashed line The values that were extracted from the model are represented in Table 4-3 Now that the modes that limit the bandwidth are identified digital filters can be derived to attenuate them

**Digital Filtering**

Digital filter processing is based on processing digitally sampled signals Digital filters are separated into two types finite impulse response (FIR) and infinite impulse response (IIR) For the FIR filter the output depends only on the input The output of an IIR filter depends both on the input series and past values of the output series The IIR

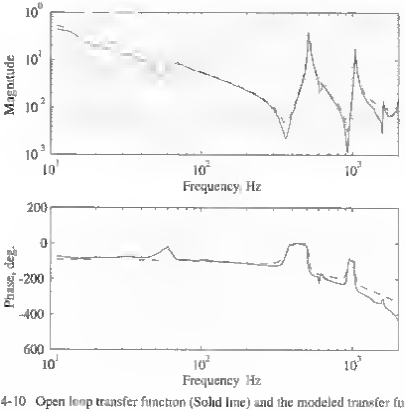


Figure 4-10 Open loop transfer function (Solid line) and the modeled transfer function (dashed line)

filter is chosen for removing the undesirable structural modes from the transfer function A short description of the filters is given in Appendix B.

Table 4 3 Parameters evaluated from experimental measurements

| | | |
|---|---|---|
| $k_1$ | 3 80e5 Nm/rad | Stiffness of mode 1 |
| $\omega_{n1}$ | 3220 rad/s | Natural frequency of mode 1 |
| $\zeta_1$ | 0 02 | Damping ratio of mode 1 |
| $k_2$ | 1 52e6 Nm/rad | Stiffness of mode 2 |
| $\omega_{n2}$ | 6570 rad/s | Natural frequency of mode 2 |
| $\zeta_2$ | 0 02 | Damping ratio of mode 2 |

Digital filters are needed to attenuate the structural modes. Digital filters can be introduced anywhere in the digital part of the control loop. Three different filters were chosen to improve the feed drive performance. Figure 4-11 shows two of these positions, the velocity loop filter and the position loop filter. The velocity loop filter $H_v(z)$ is installed inside the velocity loop and is used to filter the two main torsional modes. The position loop filter $H_p(z)$ is installed outside the velocity loop and inside the position loop its purpose is to clean anything left untreated in the closed velocity loop. A third filter is placed outside the position loop. That type of filtering is called feedforward filtering since it does not affect the feedback loop. Feedforward can be used to improve on the system by altering the commanded motion and it does not affect stability. The implementation of feedforward is described in Chapter 7.

The objective of the digital filters is to cancel the two torsional flexibilities. Each mode is represented by two poles and two zeros near the unit circle in the z-plane. The digital filter theoretically uses poles to cancel structural mode zeros. Likewise, the filter

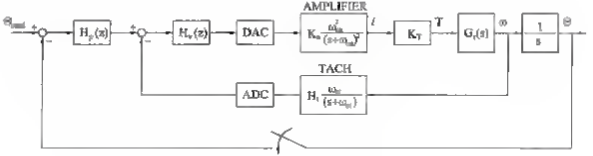


$H_p(z)$ Position loop compensation

$H_v(z)$ Velocity loop compensation

Figure 4-11 Position loop block diagram

uses zeros to cancel structural mode poles The result should equal one. It is possible to design an unstable filter if the filter poles are matched to zeros that are outside the unit circle Consequently the poles are placed as close as possible to the zeros but in the unit circle The representation of the digital filter is described in the following equation,

$$H_{scmp}(z) = \frac{1-[2r_{zl}\cos\Theta_{zl}]z^{-1}+r_{zl}^{2}z^{-2}}{1-[2r_{pl}\cos\Theta_{pl}]z^{-1}+r_{pl}^{2}z^{-2}} \qquad (4\text{-}7)$$

The poles and zeros are described by $r$ the radius from the center and $\Theta$ the angle $H_{scmp}(z)$ is the transfer function for one sets of poles and zeros

Table 4-4 shows how the poles of the system are the zeros of the filter and how the zeros are now the poles. The same open loop sine sweep test is performed with the filters implemented Figure 4-12 shows the compensated open-loop transfer function. Both peaks from the previous measurement are now removed, therefore the velocity loop can be closed with the highest possible gain Once the velocity loop is tuned to the best achievable gain $K_{vs}$ a transfer function is measured by applying a similar sine sweep test Figure 4-13 shows the compensated velocity loop of the system. The bandwidth of the velocity loop is around 200 Hz with a phase shift of 100 degrees at 200 Hz The 50 Hz mode remains although it does not affect the stability of the system Several attempts to remove it in the position loop filter $H_p(z)$ failed because the mode is non linear As the table traverses the rails the natural frequency of the that mode changes

The position loop is closed without any filters added to it Figure 4-14 shows the transfer function of the position loop between the input and the encoder as an output The position loop reached around 100 Hz although the notch due to the 50 Hz mode did deteriorate the performance The 100 Hz is achieved with the highest possible position

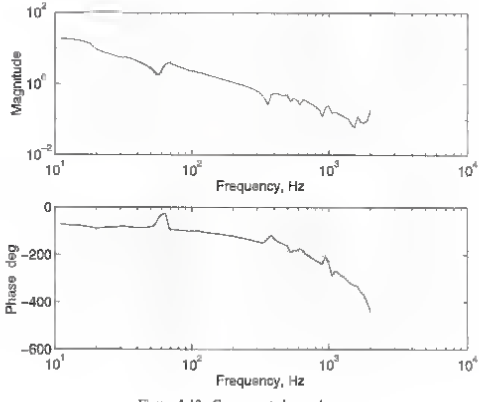


Figure 4-12 Compensated open loop

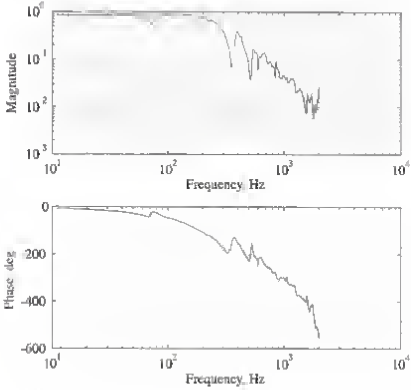


Figure 4 13 Compensated velocity loop as seen from tachometer

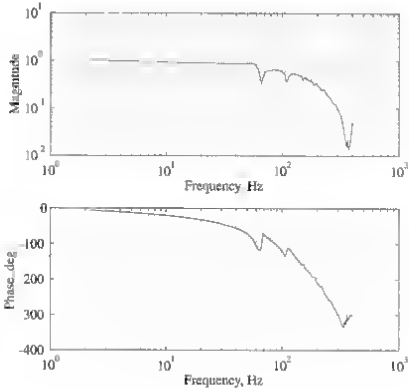


Figure 4-14 Closed Position loop

loop gain The gains are reduced in the final implementation as a safeguard against unforeseen changes in the machine performance producing instability The current bandwidth after this safeguard is 70 Hz

Table 4-4 Compensation poles and zeros

| Poles and zeros of $G_{vp}(z)$ | | | | Poles and zeros of $H_1(z)$ | | | |
|---|---|---|---|---|---|---|---|
| Poles | | Zeros | | Poles | | Zeros | |
| Radius | Angle | Radius | Angle | Radius | Angle | Radius | Angle |
| 0.98588 | +0.7108 | 0.97319 | +0.5101 | 0.97319 | +0.5101 | 0.98588 | +0.7108 |
| 0.98588 | -0.7108 | 0.97319 | -0.5101 | 0.97319 | -0.5101 | 0.98588 | -0.7108 |
| 0.97139 | +1.4508 | 0.95871 | +1.2329 | 0.95871 | +1.2329 | 0.97139 | +1.4508 |
| 0.97139 | -1.4508 | 0.95871 | -1.2329 | 0.95871 | -1.2329 | 0.97139 | -1.4508 |

After the position loop is closed some motion commands are performed to show the performance of the machine Figure 4-15 shows a 2 inch (50800 cts) move at a feedrate of 200 in/min and a 1 g acceleration Figure 4-16 shows the steady state error of the system The steady state error could be better seen in the following plot Figure 4-17 which shows that the following error is about 500 counts (0.02 inches) This error only shows that the actual position is lagging behind the commanded position by 0.02 inches It is equivalent to a time delay Since it is a constant during steady state motion it should not affect the accuracy of the part This lag error is only significant on machined parts when several axes are commanded to make a coordinated move For instance, if each axes has a different time delay between the command and the actual position, a circular move will be actually elliptical Tuning all axes to have similar following errors is not possible since they have different components Feedforward is later applied to reduce these errors

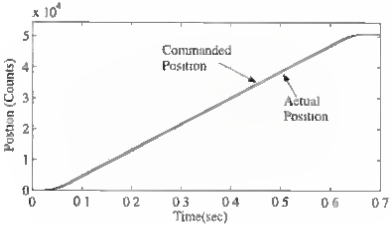


Figure 4-15 Commanded and actual motions

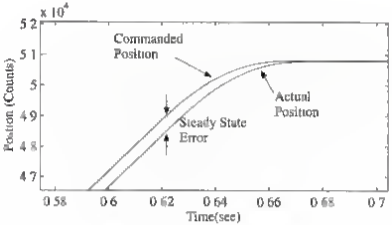


Figure 4-16 Zoomed detail of the commanded and actual motions of the ballscrew drive

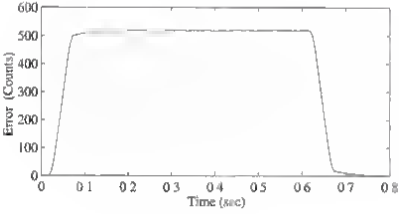


Figure 4 17 Following error

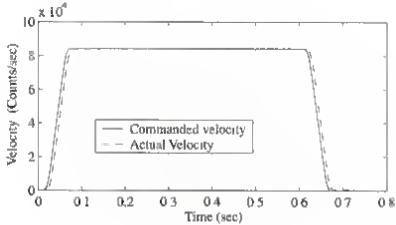


Figure 4-18 Velocity profile

It is evident that with careful tuning and good understanding of a system a wide bandwidth is possible on ballscrew drives. The use of digital filters has increased the bandwidth of a ballscrew drive from 30 Hz to 100 Hz. This more than triples the maximum acceleration.

# CHAPTER 5
# HIGH BANDWIDTH USING SLIDING MODE CONTROL

The digital filters inserted in the PID loop suffer from the lack of robustness. The filters were designed to exactly fit the measured transfer function. If there are any changes in the transfer function the filters will stop cancelling the poles and zeroes and they will cause an instability. A sliding mode controller is a robust controller that should provide high bandwidth.

The sliding mode controller (SMC) is a control algorithm that can offer excellent trajectory tracking without the need for precise system modeling. In many real world applications, it is not an easy task to precisely model or define the system parameters. The sliding mode controller can also compensate for external disturbances like cutting forces and friction. The theory of the sliding mode controller first appeared in the former Soviet Union in the 1950s. Since then several researchers have modified it to improve its performance.

## Sliding Mode Theory

The single input single-output (SISO) sliding mode controller described here is based on the work of Slotine [17]. Consider the system in Equation 5-1:

$$x^{(n)} = f(X) + B(X)u \tag{5-1}$$

where $x$ is the desired output, $u$ is the control input, $X$ is the state vector, $\hat{B}(X)$ represents the input gain and $\hat{f}(X)$ represents the system dynamics. If $\hat{f}(X)$ is the estimated system dynamics then Equation 5-2 represents the uncertainty in the system dynamics

$$\left|\hat{f} - f\right| = F \tag{5-2}$$

where $F$ is the upper boundary for the system uncertainty

The purpose of this controller is to force the state $X$ to track a desired state $X_d$ in the presence of disturbances and system uncertainties. Equation 5-3 is the tracking error vector

$$X = X - X_d = [\tilde{x}\ \dot{\tilde{x}}\ \ddot{\tilde{x}}\ \ldots\ \tilde{x}^{(n-1)}]^T \tag{5-3}$$

Furthermore, the sliding mode controller requires high speed switching of the control effort to drive the plant on a time varying surface $S(t)$ in state space $\mathbb{R}^{(n)}$. Tracking $X = X_d$ is equivalent to that of remaining on the time varying surface (or sliding surface) for all $t > 0$. Although there are several ways to represent the sliding surface, the most common representation is Equation 5-4

$$s(x,t) = \left(\frac{d}{dt} + \lambda\right)^{n-1} \tilde{x} \tag{5-4}$$

where $s(x,t)$ is the scalar representation of the sliding surface, $\lambda$ is a user chosen parameter greater than zero, and the term $n$ is the system order.

For example, Equation 5-5 represents a second order system

$$\ddot{x} = \hat{f}(x, \dot{x}) + u \tag{5-5}$$

If $n = 2$ then the sliding surface is

$$s(x,t) = \dot{\tilde{x}} + \lambda\tilde{x} \tag{5-6}$$

Figure 5-1 shows the sliding surface on the phase plane. The straight line in the figure represents Equation 5-6 where $\lambda$ is the slope of the line.

Equation 5-7 represents the derivative of the sliding surface.

$$\dot{s} = \ddot{\tilde{x}} - \ddot{\tilde{x}}_d + \lambda\dot{\tilde{x}} = f + u - \ddot{x}_d + \lambda\dot{\tilde{x}} \tag{5-7}$$

The derivative of the sliding surface is also called the average of the system dynamics on both sides of the surface. When the system is in sliding mode the dynamics can be written as

$$\dot{s} = 0 \tag{5-8}$$

From Equation 5-7 and Equation 5-8, the approximated control signal is

$$\hat{u} = -\hat{f} + \ddot{x}_d - \lambda\dot{\tilde{x}} \tag{5-9}$$

In order for the system to remain on the surface the following Lyapunov function must be satisfied.

$$\frac{1}{2}\frac{d}{dt}s^2 \le (-\eta)|s| \tag{5-10}$$

where $\eta$ is strictly a positive constant. The equation states that the squared distance to the surface, measured as $s^2$, decreases along all system trajectories. This ensures that all trajectories point towards the surface $S(t)$.

A discontinuous term must be added to $u$ to satisfy the Lyapunov function. Equation 5-11 represents the discontinuity

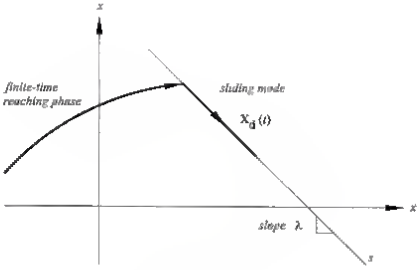


Figure 5-1 Phase plane

$$u = u - k \times \mathrm{sgn}(s) \tag{5-11}$$

where sgn is the signum function

$\mathrm{sgn}(s) = +1$ if $s > 0$

$\mathrm{sgn}(s) = -1$ if $s < 0$

The parameter $k = k(x, \hat{x})$ should be large enough to guarantee that Equation 5-10 is satisfied. From Equation 5-11, $\hat{u}$ is replaced in Equation 5-9. Then the result is combined with Equation 5-7 to yield the following equation

$$\dot{s} = [f - \hat{f} - k\,\mathrm{sgn}(s)] \tag{5-12}$$

Substitution of Eqnation 5-12 into the Lyapunov function Equation 5-10 yields Equation 5-13

$$k = F + \eta \tag{5-13}$$

Then the control law is derived in Equation 5-14

$$u = -\hat{f} + \ddot{x}_d - \lambda \dot{\tilde{x}} - k \times \mathrm{sgn}(s) \tag{5-14}$$

A problem with the control law in Equation 5-14 is that it is discontinuous along the surface. The high speed switching causes the system to chatter along the surface. This chattering leads to undesirable high control activity and excites high frequency dynamics in the system that were neglected in the model.

A thin boundary layer along the switching surface $S(t)$ is used to smooth the discontinuity. Figure 5-2 shows the boundary layer along the sliding surface. The boundary layer is described by its width $\varepsilon$ and thickness $\varphi$.

To ensure that the signal is continuous and inside the boundary layer the sgn (s) term in Equation 5-14 is replaced by the saturation of $s/\varphi$ in Equation 5-15

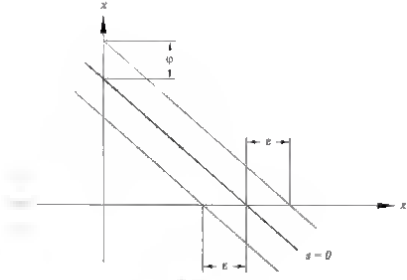


Figure 5.2 Boundary layer

$$u = \hat{u} - k\left[sat\left(\frac{s}{\varphi}\right)\right] \tag{5-15}$$

where

$sat(s) = s$ if $(|s| \leq 1)$

$sat(s) = \text{sgn}(s)$ otherwise

The thickness of the boundary layer $\varphi$ changes with time but in this case it is set as a constant parameter to simplify the calculations

**Applying a Sliding Mode**

A sliding mode controller will be further developed for the ballscrew drive case Figure 5-3 shows the open loop block diagram of the ballscrew drive. The system was modeled for only a second-order system The dynamics due to the ballscrew flexibility were not included in the model and are considered as an uncertainty

The control signal $u$ is the command from the SMC while $x$ is the position measured in counts. $T_d$ is the disturbance torque coming from the cutting forces and friction $K_a$ and $K_t$ are gains $J$ is the inertia of the screw and motor $B$ is the viscous friction in the motor and $r_g$ is the ballscrew ratio Equation 5-16 represents the algebraic form of the above block diagram,

$$\frac{J}{K_a K_t r_g}\ddot{x}(t) + \frac{B}{K_a K_t r_g}\dot{x}(t) = u(t) - \frac{1}{K_a K_t}T_d(t) \tag{5-16}$$

Rearranging Equation 5-16 results in the following equation

$$J_e\ddot{x}(t) + B_e\dot{x}(t) = u(t) - d(t) \tag{5-17}$$

where $d(t) = \frac{T_d(t)}{K_a K_t}$, $J_e = \frac{J}{K_a K_t r_g}$ and $B_e = \frac{B}{K_a K_t r_g}$

The acceleration in the drive can then be expressed as

$$\ddot{x} = \frac{1}{J_e}(-B_e\dot{x} + u - d) \tag{5.18}$$

The external disturbance $d$ caused by the cutting forces and the friction is considered a known value that remains between upper ($d^+$) and lower ($d^-$) limits which are measured on the machine. The disturbance can then be tracked using the following observer function

$$\tilde{d}(k) = \tilde{d}(k-1) + \rho\kappa sT \tag{5.19}$$

where $\tilde{d}$ is the estimated disturbance, $\rho$ is an adaptation parameter ($\rho$ =10~50), $T$ is the control period, and $\kappa$ is used to impose limits on the disturbance,

$$\kappa = \begin{cases} 0 & \text{if}(\tilde{d}(k) \le d^-) \quad \text{and}(S \le 0) \\ 0 & \text{if}(\tilde{d}(k) \ge d^+) \quad \text{and}(S \ge 0) \\ 1 & \text{otherwise} \end{cases} \tag{5.20}$$

The sliding surface is defined as a second order system and the control law is defined by Equation 5-21

$$u = J_e[\dot{\lambda}(x_d - x) + \ddot{x}_d] + B_e\dot{x} + \tilde{d} + ksat(s) \tag{5.21}$$

Figure 5-4 shows the block diagram of the sliding mode controller as it is implemented on the HSM1. A computer simulation using SIMULINK shows the commanded and actual simulated positions in Figure 5-5. The 50 800 count command is equivalent to a move of 2 inches. The feedrate is set at 200 in/min and the acceleration is set at 1 g. The value for $\lambda$ is chosen arbitrarily while the value of $k$ is calculated

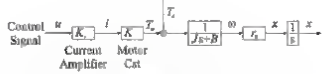


Figure 5-3 Simplified model of the axis dynamics

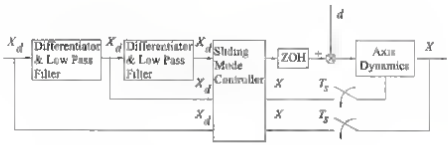


Figure 5-4 Block Diagram of the Sliding Mode Controller

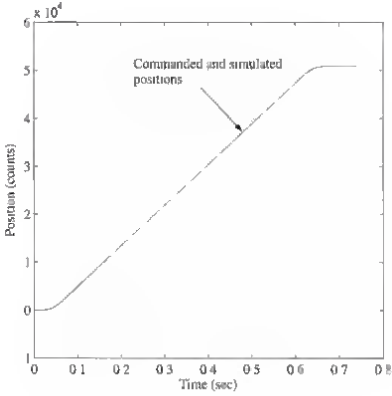


Figure 5 5 Commanded and actual simulated positions

The maximum error between the commanded and actual simulated positions occurs during the acceleration period and is equal to 60 counts.

Figure 5-6 shows the commanded and actual simulated velocities. The SMC kept the error between the commanded and actual simulated velocities to a minimum of 2,000 count/s.

The SMC is then implemented on the y axis of HSM1. The tachometer and encoder are used for feedback. The controller is used to generate the position, velocity and acceleration commands. Figure 5-7 shows the results from a move of 50,800 counts. The system is stable. A variety of position, velocity and acceleration commands were tested, and they all resulted in stable responses.

The maximum error between the simulated and actual position occurred during the acceleration period of the move. Figure 5-8 is a close up of the commanded and actual positions. Although the 150 count error during the deceleration phase is smaller than that in the acceleration phase it is more detrimental since it will cause an overshoot. In order to remove some of the error different values for $k$ and $\lambda$ were tested, but none of them yielded better results. The magnitude of the error decreased with lower acceleration commands.

The drive was estimated as a second order system to simplify the calculations; this simplification causes SMC to minimize velocity and position errors, but not acceleration errors. A third order system will minimize the acceleration error and may offer better tracking.

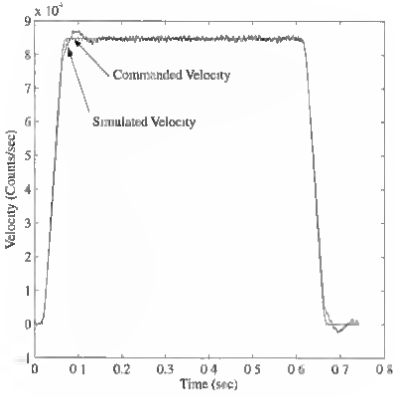


Figure 5-6. Commanded and simulated velocities

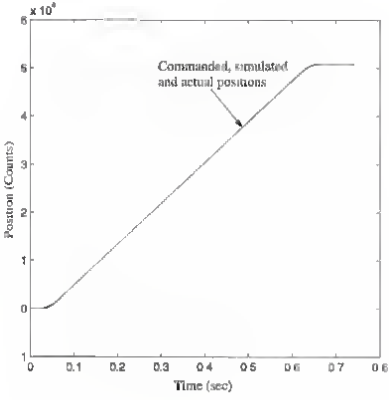


Figure 5-7 Commanded and actual positions measured on HSM1

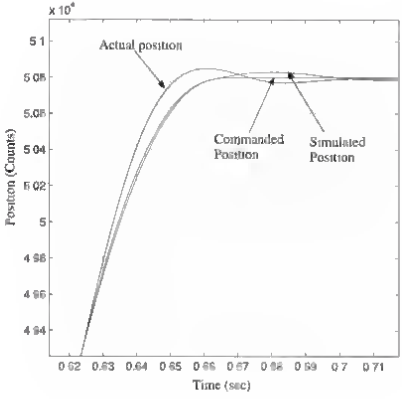


Figure 5-8 Commanded and actual positions

The bandwidth of the system is 65 Hz which is lower than the 100 Hz achieved on this drive previously using the PID with digital filters. Increasing the $\lambda$ term to increase the bandwidth of the drive results in chattering

Figure 5 9 shows the commanded and actual velocities measured on the drive The maximum error is measured at 7 000 count/s, more than three times that of the simulation The actual velocity measured from the tachometer also has more noise than anticipated

Figure 5 10 shows the difference between the implemented SMC and the existing PID tuning on the machine. The SMC slides towards the commanded position minimizing the error

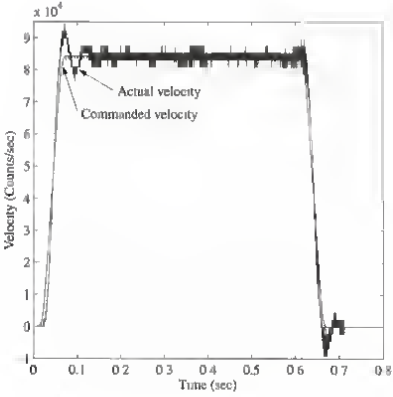


Figure 5-9 Commanded and actual velocities measured on HSM1

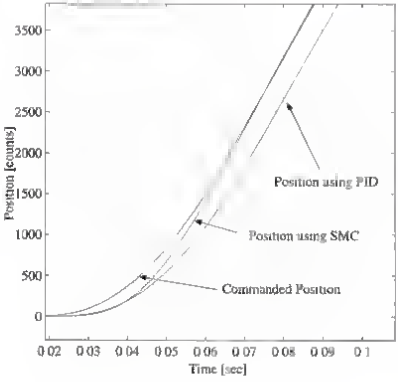


Figure 5-10 SMC vs PID loop tuning

# CHAPTER 6
# TUNING LINEAR MOTOR DRIVES FOR WIDE BANDWIDTH

Linear motors do not have the same dynamic limitations that ballscrew drives have. Linear motors are not limited by lowly damped second-order natural modes that are associated with the ballscrew mechanism; therefore, linear motors are capable of high speed and high acceleration operation. PID controllers are usually sufficient for providing high bandwidth on linear motors. Since linear motors are direct drives, they produce high accelerations; however, this also makes them sensitive to external disturbances. The two disturbances that act on linear motors in milling are the friction coming from the guideways and forces coming from the cutting tool engaged in the material. The linear motor is also sensitive to changes in mass and may become unstable with substantial changes. Modifications to the PID controller like friction feedforward and high gain can overcome external disturbances, but the system lacks the robustness to compensate for mass changes. With all these problems, a PID was still acceptable in this case because the axis selected for this analysis has a fixed mass and the cutting forces in this direction are minimal.

At the MTRC, two brushless DC ironless linear motors have been incorporated on the Z-axis of the HSM1. Figure 6-1 shows the Z-axis mounted on two pedestals. Each pedestal has a linear motor, a linear encoder, and a guideway. All the components are mounted next to each other on the top surface of each pedestal. The Z table which carries the AB-head and spindle is mounted on anti-friction, high stiffness roller bearing

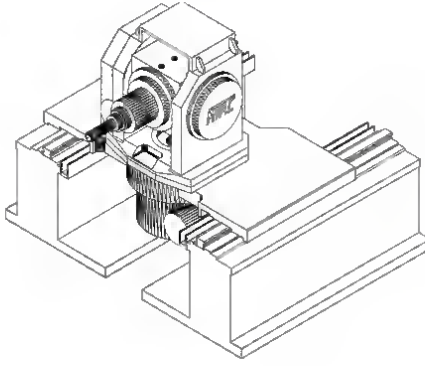

Figure 6-1 Linear motors on HSM1 Z-axis

carriages that ride on these guideways The motor configuration is such that the magnet assembly is stretched along the entire length of the travel and are stationary The short rotor is mounted to the moving table and is constrained to move between the magnet tracks The encoder is mounted next to the motor and special care in the design was taken to eliminate the use of any flexible components between them A more detailed description of the linear motor feed drive system follows

**Analysis of linear motor drive**

Each of the Trilogy LM410-4 brushless DC linear motors provided a peak force of 2 000 N The mass of the table and spindle was about 900 Kg The AB head was not mounted on the Z-axis during this analysis of the feed drive. The maximum possible acceleration was about 0 45 g.

Two Advanced Motion Control (A M C) amplifiers are used to power the linear motors These PWM amplifiers were sized to provide the maximum motor thrust force Additionally the PWM frequency was high enough not to interfere with the motor control

Two Heidenhain LS183 incremental linear encoders provided the feedback – one for each motor The encoders resolution is 4 counts/μm The encoders are also limited to a 500 mm/s maximum velocity which is the maximum velocity of the Z-axis Software compensation tables are installed on the Z axis to compensate for any yaw between the two encoders this prevents the two motors from fighting each other and burning out

The same Delta Tau controller used for the ballscrew drive was used to control the Z-axis except no additional DSP board was added The controller samples the encoder and uses the same signal to provide the position loop feedback and after the signal is differentiated the velocity loop feedback. A velocity loop signal is essential in any feed

drive servo control The signal is used to provide adequate damping for the system to prevent the drive from oscillating around the commanded position Equation 6-1 shows how the signal is generated by differencing two consecutive position samples and dividing them by the sampling time.

$$\dot{X} = \frac{X(n) - X(n-1)}{T_s} = \frac{\Delta X}{T_s} \tag{6-1}$$

A block diagram of the PD (Proportional-Derivative) control system of the Z axis is shown in Figure 6-2 This block diagram describes the different components on the feed drive. The block diagram in Figure 6-3 replaces each block element with the appropriate transfer function For example, the table block which represents the moving mass of the Z-axis table is modeled as a simple second-order system with an acceleration that is proportional to the force applied to the table This block diagram has both discrete and continuous block elements Either the discrete elements must be converted to continuous elements or the continuous to discrete to be able to analyze the system

Analysis of the block diagram requires expressing the discrete time elements as their equivalent continuous functions as shown in Figure 6-4 This reduces the entire block diagram to a continuous transfer function shown as Equation 6-2

$$\frac{X_{Actual}}{X_{Commanded}} = \frac{214K_p}{Ms^2 + 1.676T_sK_pK_ds + 214K_p} \tag{6-2}$$

The transfer function indicates that the table response depends on the mass $M$ of the table the servo period $T_s$, the proportional gain $K_p$ and the derivative gain $K_d$ The servo-period is set to 221 µs, and the mass is a constant value The only variables are the proportional gain and the derivative gain

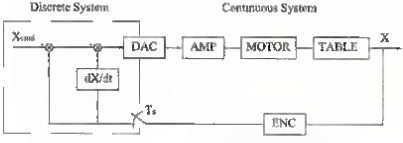


Figure 6-2 Block diagram of the Z-axis position loop

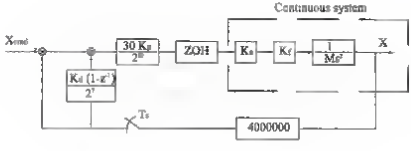


Figure 6-3 Discrete time block diagram of the Z-axis position loop

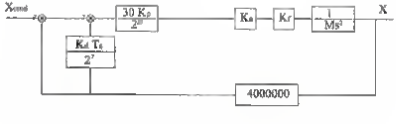


Figure 6-4 Continuous time block diagram of the Z-axis position loop

Tuning the PD controller requires an initial guess for $K_p$ and $K_d$. Equation 6-2 can be written in the second-order form of Equation 6-3 where $\omega_n$ is the natural frequency and $\zeta$ is the damping ratio of the system response. Furthermore, if $\omega_n$ is defined in terms of the rise time $T_r$ as shown in Equation 6-4, then $K_p$ and $K_d$ can be expressed as characteristics of the response to a step input as shown in Equation 6-5 and Equation 6-6.

$$\frac{X_{Actual}}{X_{Commanded}} = \frac{\omega_n^2}{s^2 + 2\zeta\omega_n s + \omega_n^2} \tag{6-3}$$

$$T_r = \frac{\pi - inv\left(\tan\left(\frac{\sqrt{1-\zeta^2}}{\zeta}\right)\right)}{\omega_n\sqrt{1-\zeta^2}} \tag{6-4}$$

$$K_p = \frac{\omega_n^2}{214M^{-1}} \tag{6-5}$$

$$K_d = \frac{2\zeta\omega_n}{1676K_pT_s} \tag{6-6}$$

With a desired damping ratio of 0.7 and 10ms rise time the gains are derived and applied to the system. The initial gains were too high and caused the motors to emit a high-pitched hum. Iteratively the rise time was relaxed while the damping ratio remained constant. After the hum had been attenuated with a 500 Hz low-pass filter and the position loop had been tuned, the transfer function of the system was measured. From Figure 6-5 the resultant transfer function shows a 70 Hz bandwidth.

The high-pitched hum emitted from the motor occurs when the gain in the velocity loop is too high. The velocity loop feedback is being generated digitally from the position loop feedback. This calculation introduce noise into the system. Pritchow [13] suggests

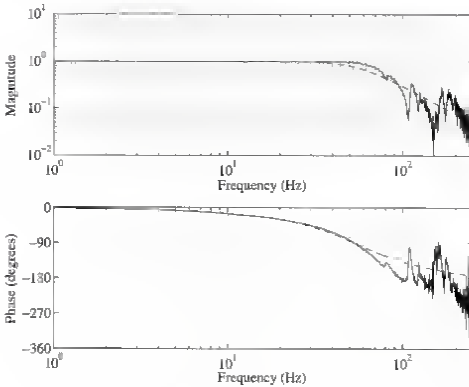


Figure 6-5 Actual (solid line) and modeled (dashed line) Closed loop frequency response of the Z-Axis using linear motors

two methods to remove this noise The first suggestion is to oversample the feedback signal and use averaging filters to smooth the velocity loop feedback The second suggestion is to introduce a Ferraris feedback sensor for the velocity loop

The first suggestion was evaluated on this drive but it did not produce favorable results Oversampling on the Delta Tau controller was achieved by increasing the sampling time for the position loop and keeping the sampling time for the velocity loop fixed This result improved the performance of the velocity loop but it drastically deteriorated the performance of the position loop

The second suggestion requires the introduction of an accelerometer to the system This accelerometer measures the relative velocity between the moving and fixed parts of the drive This accelerometer is commonly referred to as the Ferraris sensor The relative acceleration measured by the sensor is then integrated to provide a velocity signal Typically the velocity signal has better resolution and does not suffer from noise associated with differencing a signal Using this sensor on this linear drive is not possible because of space limitations

Currently the velocity loop is providing enough damping as shown in the step response of Figure 6 6 The system exhibits a damping ratio of 0 8 and an overshoot of 5% The response shows that the motor is suffering from an external disturbance in this case it is friction from gudeway covers

**External Disturbances in Linear Motor Drives**

Up to this point, the linear motor drive could position to within 20 counts (5μm) Reduction of the steady-state error was achieved by the addition of integral gain to the controller The integral gain successfully dropped the steady state error to one count In

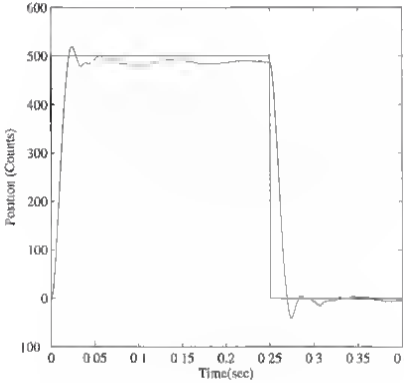


Figure 6-6 Step response of the linear motor drive

addition, integral gain provided much needed stiffness to the drive. Static stiffness is measured by applying a constant load to the drive while the actual position is sampled.

Figure 6-7 shows the PD controller under a 200 N static force. The force was increased from 0 N to 200 N over a period of one second. The PD controller shows an error of 2.8 μm, which equates to a static stiffness of 0.014 μm/N. Under PID control, the error was eliminated which leads to the conclusion that the static stiffness under PID is infinite after after the response settled and as long as the force is within the thrust capacity of the motor. Unfortunately, integral gain can also lead to drastic errors during motion. Integral gain acts on the drive upon sensing an error between the commanded position and the actual position. It is most useful for correcting errors at the end of each motion.

As an example, the linear drive was commanded a motion under PD and PID control. Figure 6.8 shows the tracking error which is the difference between the commanded and actual position of the drive. The errors measured in the PD loop are all constant and they are mainly due to a time delay between the commanded motion and the actual motion. This time delay does not show up as an error on the parts. It only means that the tool will follow the commanded path but arrive at the end late. Under PID control, the time delay is not constant anymore. The integral gain senses that there is a huge error and attempts to correct for it. This correction causes a distortion in the motion.

During machining several axes of the machine move simultaneously. If each one of them has a different time delay this results in distorted motions. Circles become ovals and corners become rounded. A fixed and equal time delay on all axes is necessary to produce good parts. Since the machine has different axes that are made from different motors and amplifiers, it becomes a challenge to linearize and match all time delays.

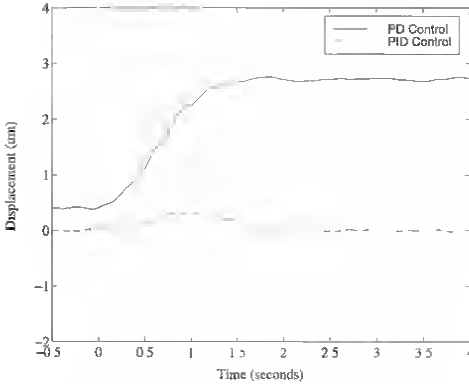


Figure 6-7 Response of the linear drive to a 200 N force disturbance

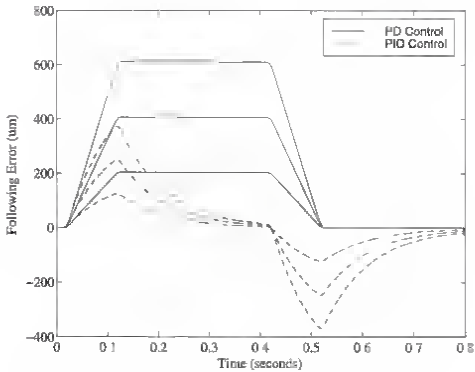


Figure 6.8 Commanded and actual tracking errors using both PD and PID control

Minimizing the time delay or removing it completely is a preferred option. One method of removing the following error or time delay is feedforwarding the commanded motions. Implementation of a feedforward filter is given in the following chapter.

# CHAPTER 7
# FEEDFORWARD FILTERS

CNC machining of complex geometries involves the simultaneous motion of several axes. In the case of HSM1, it may involve the motion of all five axes. Each of these axes has different mechanical and electrical properties. The X and Y are ballscrew driven, the Z is linear motor driven, and the AB head uses rotary motors and worm gear transmission for both axes. Each of these five axes performs differently--but when they work together they, need to behave similarly to reduce part defects. In point-to-point motions, the tracking error does not cause any actual machining errors, but in multi-axis machining, the difference in following errors between axes causes part defects.

For example, when machining a circle, both feed drive axes are commanded through a sine wave profile with one wave shifted by $\pi/2$. At any given time, the position of each axis must be on the wave to perform a perfect circle. Figure 7-1 shows a perfect circle as a solid line. When the axes have different delays then the circular becomes distorted as shown as a dotted line. To correct the distortion requires that the tracking error on both axes be the same. With very different axes, this is not possible because they behave differently. Feedforward filters are suggested for removing these errors.

Feedforward filters have been the subject of several researchers. Tomizuka [6] and Weck [5] both investigated the subject. Their investigations were discussed in Chapter 2. These filters essentially modify the command to counter-act system dynamics and feedforward it to the system in order to reduce the amount of the tracking error.

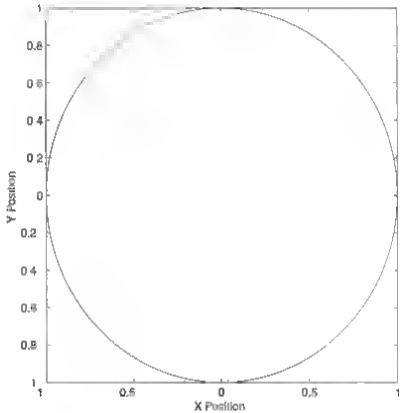


Figure 7.4 Circular motion with two different time delays in the Y direction

**Feedforward Filter Analysis**

The purpose of the feedforward filter is to minimize the tracking error between the commanded motion and the actual motion of the feed drive. Figure 7-2 shows a block diagram of a servomechanism under PD control. The tracking error is $E(z)$. The objective of the feedforward filter $H_{ff}(z)$ is to reduce the tracking error to zero. Equation 7-1 is the algebraic equivalent of the block diagram in Figure 7-2.

$$E(z) = X(z) - H(z)[K_p E(z) - K_v G(z)Y(z) + H_{ff}(z)X(z)] = 0 \tag{7-1}$$

Solving for the filter will result in Equation 7-2.

$$H_{ff}(z) = H^{-1}(z) + K_v G(z) \tag{7-2}$$

The feedforward filter is the inverse of the open loop transfer function $H(z)$ and the velocity loop feedback. This assumes that Equation 7-3 is the representation of a servomechanism drive. Equation 7-4 is the discrete time equivalent of a differentiator using Tustin's method.

$$H(z) = \frac{1}{2}KT_s^2 \frac{z+1}{(z-1)^2} \tag{7-3}$$

$$G(z) = \frac{2(z-1)}{(z+1)} \qquad \text{(Tustin's method)} \tag{7-4}$$

Substituting Equation 7-3 and Equation 7-4 in Equation 7-2 results in Equation 7-5.

$$H_{ff}(z) = \frac{2K_{aff}(z-1)^2}{z+1} + \frac{2K_{vff}(z-1)}{z+1} \tag{7-5}$$

where $K_{aff}$ and $K_{vff}$ are,

$$K_{aff} = 1/(KT_s^2) \qquad K_{vff} = K_v \tag{7-6}$$

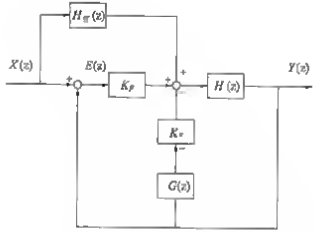


Figure 7-2 Discrete time PID with feedforward

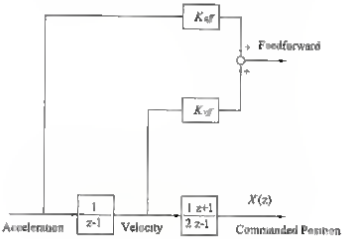


Figure 7-3 Feedforward filter

The two terms $K_{aff}$ and $K_{vff}$ are referred to as the acceleration and velocity gains of the feedforward filter. The acceleration gain modifies the acceleration part of the profile and the velocity terms modify the velocity part of the profile. For programming Equation 7-6 in the control loop, the acceleration and velocity are calculated from the trajectory generator. Figure 7.3 shows how the two terms are calculated from the command.

**Feedforward on Leadscrew Drives**

The closed position loop of the ballscrew drive is shown in Figure 7-4. The feedforward filter is installed ahead of the position loop and alters the command to produce the desired motion. The values for the velocity and acceleration feedforward gains are calculated and applied to the ballscrew drive.

The tracking error was reduced on a simulated system. Figure 7.5 shows the tracking error of a PD system without the filter. The error is 750 counts. With the feedforward filter, the error drops to one count except during the acceleration phase of the motion where it is about 5 counts as shown in Figure 7.6.

This same filter was applied to the ballscrew drive of the machine and the results were similar. The filter reduced the error to less than one count. Figure 7.7 and Figure 7.8 show the errors on the ballscrew drive of the Y axis on HSM1.

**Feedforward on Linear Motor Drives**

Similarly the feedforward filters are applied to the linear motor drive of HSM1. The filters were used with a PD controller and a PID controller. Figure 7.9 shows how the reduction in tracking error by using feedforward filters on the linear motors. The

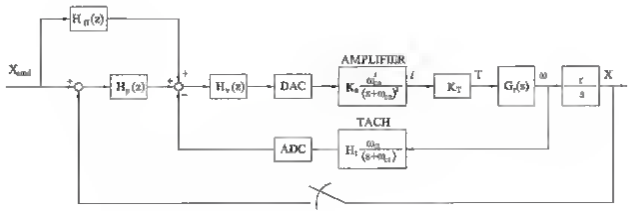


$H_p(z)$ Position loop compensation
$H_v(z)$ Velocity loop compensation
$H_{ff}(z)$ Feedforward filter

Figure 7-4 Block diagram of ballscrew drive with feedforward

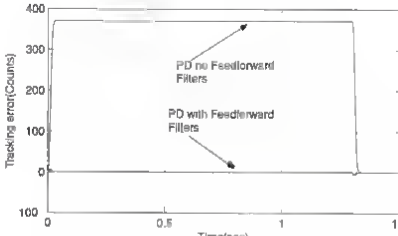


Figure 7 5 Simulated tracking error of a PD with and without feedforward filters

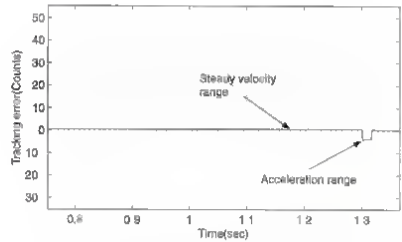


Figure 7-6 A more detailed look of the simulated tracking error with feedforward filters

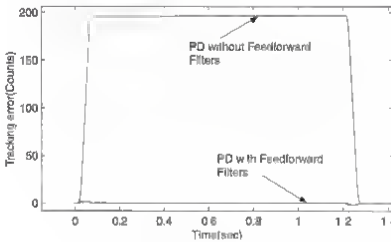


Figure 7-7 Actual tracking error on the ballscrew drive

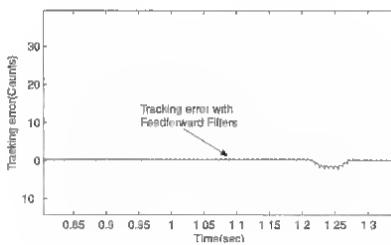


Figure 7-8 A closer look on the actual tracking error of the ballscrew drive

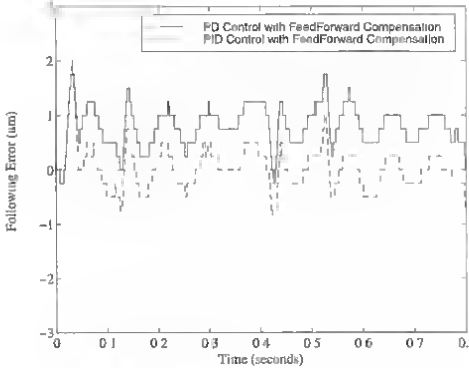


Figure 7-9. Tracking error for the linear motors using PD and PID controllers

tracking error during steady velocity is 1µm (4 counts) using a PD controller and is a maximum of 2 µm (8 counts) In the acceleration part of the motion With PID the tracking error is 0 5 µm (2 counts) during steady velocity and is 2µm (8 counts) during the acceleration part of the motion

**Summary**

In summary the feedforward filter reduces the tracking error tremendously Therefore the corrected multi axis motions will not create machining significant defects due to time delays between the commanded and actual motion

# CHAPTER 8
# CONCLUSIONS

The selection of a linear motor drive over a ballscrew drive simply because linear motors can achieve higher bandwidth with a PID controller is not good design practice. There are advantages and disadvantages in both designs and proper selection should be based on the evaluation of all the limitations as they apply for each particular machine. On one hand, ballscrew drives have limited speeds and accelerations, but with digital filters or a more robust controller, the acceleration can be increased by widening the bandwidth. On the other hand, linear motor drives can achieve high bandwidth with a simple PID controller but suffer from sensitivities associated with direct drives like changes in mass and external forces.

## Ballscrew Drives

The major disadvantage in a ballscrew drive is its limited bandwidth due to lowly damped second-order dynamics associated with the ballscrew. These dynamics can be attenuated with digital filters inserted in the velocity loop of a PD controller. These filters are complicated to design and implement because they have to match system dynamics. If for any reason the system dynamics change the digital filters will not be able to attenuate the new dynamics, and furthermore the filters will act as a source of instability.

A more robust sliding mode controller can achieve a higher bandwidth without accurate modeling. The sliding mode controller can cope with any uncertainties within its

boundary layers The disadvantage of this controller is setting acceptable boundary layers These layers are a compromise between uncertainties and performance. Relaxing the boundaries for uncertainties decreases performance Conversely tightening the boundary layers increases performance but may cause system instability

**Linear Motor Drives**

The advantage in using a linear motor drive is that they are easily tuned to achieve a high bandwidth Linear motors can reach speeds and accelerations that surpass ballscrew drives because they are kinematically simpler The disadvantage of linear motors is that they are sensitive to disturbances The performance of a PID controlled linear motor drive is incapable of coping with large changes in the moving mass Sufficient changes may lead to instability Another disadvantage to linear motor drives is the effects of cutting forces and friction because these are not suppressed by a transmission ratio Because these forces are generally not constant but are continuously applied, the continuous force of the motor must be sized to be greater than the sum of the cutting forces and friction

Additionally both linear motor drives and ballscrew drives have time delays between the commanded and actual motions These time delays are usually kept constant to minimize errors This is not possible for linear motors because they need integral gain to increase their stiffness and to help them overcome external disturbances Integral gain causes a non-uniform time delay Feedforward filters are added on all the axes to remove the time delay

**Feedforward Techniques**

Feedforward filters were used to improve tracking of ballscrew drives and linear motor drives under PD and PID control. These filters were capable of decreasing most of the tracking error

# APPENDIX A
# MACHINE PARAMETERS

Table A-1 Linear motor parameters [18]

| MOTOR MODEL | Units | LM410-4 |
|---|---|---|
| Number of poles | | 4 |
| CoilLength | in (mm) | 14 56 (369 8) |
| Coil weight | lbs (kg) | 6 50 (2 95) |
| Magnet trackweight | lb/ft (kg/M) | 20 0 (29 8) |
| Force constant | lb/A (N/A) | 23 0 (102 3) |
| Coil resistance Ph Ph | ohms | 15 3 |
| Continuous force (coil at 75 EC rise) | lbs (N) | 90 (400) |
| Continuous power | watts | 226 |
| Peak force | lbs (N) | 450 (2000) |
| Peak power | watts | 6700 |
| Peak current | A | 18 4 |
| Continuous current | A | 3 7 |
| Heat Dissipation constant (no cool) | watts / °C | 3 0 |
| Heat Dissipation constant (air cool) | watts / °C | 3 66 |
| Heat Dissipation constant (liquid cool) | watts / °C | 4 50 |
| Inductance | mh | 20 0 |
| Back emf | V/in/sec | 2 40 |

Table A-2. Linear motor amplifier [18]

| Amplifier model | Units | S30A40AC |
|---|---|---|
| AC supply voltage | VAC | 480 3-Phase |
| Continuous DC current available from<br>internal power supply | A<br>A | 30 A for Three Phase AC Input<br>15 A for Single Phase AC Input |
| Peak DC current available from<br>internal supply (Max. 2 Seconds) | A<br>A | 60 A for Three Phase AC Input<br>30 A for Single Phase AC Input |
| Internal shunt resistor | ohms | 30 @ 50 W |
| Shunt switch-on voltage | V | 390 |
| Bus capacitance | $\mu$F | 1980 |
| Shunt fuse | A | 3 @ 250 VAC |
| AC line fuses | A | 15 @ 250 VAC |

Table A-3 Rotary Motor Parameters [19]

| Description | Units | B-604B |
|---|---|---|
| Horse power | HP | 18 6 |
| Kilowatts | kw | 13 9 |
| Speed at rated power | RPM | 2000 |
| Max operating speed | RPM | 2000 |
| Continuous torque (stall) at 40 °C | N-m | 78 7 |
| Continuous torque (stall) at 25 °C | N m | 83 4 |
| Continuous line current | Amps RMS | 48 0 |
| Peak torque | N m | 230 0 |
| Peak line current | Amps RMS | 147 0 |
| Max. theoretical acceleration | rad/sec$^2$ | 27 400 |
| Torque sensitivity (stall) ±10 % | N m/Amp RMS | 1 646 |
| Back EMF (line-to-line) ±10 % | V/KRPM | 99 6 |
| Max line-to-line volts | Volts RMS | 250 |
| DC res at 25 °C (line to-line) ±10 % | Ohms | 0 129 |
| Inductance (line-to line) ±30 % | mh | 7.2 |
| Rotor inertia | kg m$^2$ | 0 00840 |
| Mass | kg | 50 6 |
| Static friction | N-m | 0 90 |
| Thermal time constant | Minutes | 48 |
| Viscous damping | N m/KRPM | 0 300 |

Table A-4 Rotary Motor Amplifier [19]

| Description | BDS4 255X |
|---|---|
| Main DC bus | |
| Minimum | 250 VDC |
| Maximum | 360 VDC |
| Unregulated logic bus input | 14.5-26 VDC @ 0.25 Amps |
| | 14.5 26 VDC @ 0.25 Amps |
| Fan AC line input | 95 -132 VAC @0.75 amps |
| Output current (RMS/Phase) | |
| (45 decC AMB) | (Fan Cooled) |
| Continuous (RMS) | 55.0 Amps |
| Peak (2.0 sec ) | 110 Amps |
| Output KVA (@330 VDC BUS) | |
| Continuous (45 degC AMB) | 20 KVA |
| Peak (2.0 sec ) | 40 KVA |
| Internal heat dissipation | 445 Watts |
| PWM switching frequency | 10.0 KHZ |
| Motor current ripple frequency 10% | 20.0 KHZ |
| Resolver excitation frequency | 7.0 KHZ |
| Form factor RMS/AVG | < 1.01 |
| Speed regulation (Long Term) | 0.075% / degC |
| "Minimum Controllable Speed. | |
| Standard 12-Bit R/D with 8000 RPM Max Tracking rate | 2.0 RPM |
| 12 Bit R/D with 14000 RPM Max Tracking Rate | 3.5 RPM |
| 14-Bit R/D with 2000 RPM Max Tracking Rate | 1/8 RPM |
| 14-Bit R/D with 3500 RPM Max Tracking Rate | 1/4 RPM |
| 16-Bit R/D with 500 RPM Max Tracking Rate | 1/64 RPM |

a Minimum controlled speed is defined as the maximum speed that can readily be run. The standard BDS4 is configured with a 12 bit R/D converter for a maximum motor speed of 8000 RPM

# APPENDIX B
# DIGITAL FILTERING TECHNIQUES

This is a short introduction to digital filtering. It is not intended to be a comprehensive description on digital filtering. A more thorough introduction is included in Strum and Kirk [20].

Digital filtering in digital signal processors is based on processing sampled signals. Signals are sampled at equal time intervals, which is determined by a hardware clock on the DSP board or externally from a different processor. The sampling frequency is referred to as $f_s$. The ratio of the frequency of the signal over the sampling frequency times $2\pi$ is the digital frequency $\Theta$.

Individual samples can then be obtained by indexing the sample number $n$. For example, for a given frequency $f$ and sampled frequency $f_s$ the sine wave can be evaluated from the following:

$$\sin(\Theta n) \qquad n = 0, 1, 2, 3, \ldots \tag{B-1}$$

A filter can be represented by an equation with an input $X(n)$ and an output $Xf(n)$. There are two common types of filters FIR and IIR: finite impulse response and infinite impulse response filters.

Equation B-2 describes the FIR filter.

$$Xf(n) = b_0X(n) + b_1X(n-1) + \quad + b_kX(n-k) = \left( \sum_{n=0}^{k} b_nX(n-k) \right) \tag{B-2}$$

where $k$ is the order of the filter and the b's are the filter coefficients If a delay operator, z, is defined the series can be written in terms of this delay operator as follows,

$$Xf(z) = (b_0 + b_1 z^{-1} + b_2 z^{-2} + \_ + b_k z^{-k}) X(z) \qquad (B\text{-}3)$$

The transfer function of the filter H(z) can be written as the output over the input

$$H(z) = \frac{Xf(z)}{X(z)} = (b_0 + b_1 z^{-1} + b_2 z^{-2} + \quad + b_k z^{-k}) \qquad (B\text{-}4)$$

The roots of the z polynomial in the numerator of the transfer function are known as the zeros of the transfer function

The infinite impulse response filter depends both on the input and past output values of the filter to form the output. The filtering action can be written as follows,

$$Xf(n) + \quad + a_m Xf(n-m) = b_0 X(n) + b_1 X(n-1) + \quad + b_k X(n-k) \qquad (B\ 5)$$

where the terms areas previously mentioned and the a's represents the coefficients placed on the past output of the filter This can be more compactly written as follows

$$Xf(n) = \left( \sum_{n=0}^{k} b_n X(n-k) \right) - \left( \sum_{m=1}^{km} a_m Xf(n-km) \right) \qquad (B\ 6)$$

There is a possibility that the filter can be unstable. The transfer function of the filter can be written in terms of the delay operator z as follows

$$H(z) = \frac{Xf(z)}{X(z)} = \frac{(b_0 + b_1 z^{-1} + b_2 z^{-2} + \quad + b_k z^{-k})}{(1 + a_1 z^{-1} + a_2 z^{-2} + \quad + a_m z^{-m})} \qquad (B\text{-}7)$$

The roots of the denominator polynomial are known as the 'poles' of the filter The poles must lie within the unit circle in the z plane in order for the filter to be stable

## REFERENCES


1 Zelinski P. "High Speed Machining Aerospace Boeing s One Part Harmony," *Modern Machine Shop* Vol 72 No 3 August 1999 pp 10 18

2 Smith A. 1999 "Conceptual and Stuctural Design of a High Speed Five Axis Milling Machine" M S Thesis University of Florida Gainesville Florida

3 Ogata, K., 1997 Modern Control Engineering Prentice-Hall, Upper Saddle River NJ

4 Chen Y., Tlusty J. 1995 "Effect of Low Friction Guideways and Lead Screw Flexibility on Dynamics of High Speed Machines," Annals of CIRP Vol 44/1, pp 353 357

5 Weck, M., Ye G. 1990, "Sharp Corner Tracking Using the IKF Control Strategy" Annals of CIRP Vol 39/1 pp 437-441

6 Tomizuka, M., 1987 "Zero Phase Error Tracking Algorithm for Digital Control" Journal of Dynamic Systems Measurement, and Control, Vol 109 pp 65-68

7 Yao B. Al-Majed M. Tomizuka, M., 1997 "High Performance Robust Motion Control of Machine Tools An Adaptive Robust Control Approach and Comparitive Experiments" IEEE/ASME Transactions on Mechatronics Vol 2/2 pp 63 76

8 Altintas Y. Erkorkmaz K. Zhu W. H. 2000, Sliding Mode Controller for High Speed Feed Drives Annals of CIRP Vol 49/1 pp 422-429

9 Van Brussel H. Van den Braembussche P. 1998 Robust Control of Feed Drives with Linear Motors." Annals of CIRP Vol 47/1 pp 325 328

10 Slotine, J. J. Sastry, S. S. 1983 "Tracking Control of Non-Linear Systems Using Sliding Surfaces with Applications to Robot Manipulators," International Jonrual of Control, Vol 38 no 2 pp 465-492

11 Boncher P. Dumur D. Rahumam K. F., 1990 "Generalized Predictive Cascade Control (GPCC) for Machine Tools Drives." Annals of CIRP Vol 39/1 pp. 357-360

12 Koren, Y., Lo, C.-C., 1991 "Variable-Gain Cross-Coupling Controller for Contouring." Annals of CIRP Vol 40/1 pp 371 374

13 Pritshow, G., 1998, "A Comparison of Linear and Conventional Electromechanical Drives," Annals of CIRP, Vol. 47/2, pp. 541-548.

14 Tohme, Y., 1998, "Performance of High Speed Milling Machine Feed Drives Using Rotary Servomotors," M.S. Thesis, University of Florida, Gainesville, Florida.

15 Smith, D. A., 1999, "Wide Bandwidth Control of High Speed Milling Machine Feed Drives," Ph.D. Dissertation, University of Florida, Gainesville, Florida.

16 Basak, A., 1996, Permanent-Magnet DC Linear Motors, Oxford University Press Inc., NY.

17 Slotine, J.J., Li, W., 1991, Applied Non-Linear Control, Prentice Hall, Englewood Cliffs, New Jersey, pp. 276-303.

18 Trilogy Systems, 1999, LM410 Installation Manual, Webster, TX.

19 Industrial Drives, 1993, BDS4 Series Installation and Setup Manual, Radford, VA, pp. I-17.

20 Strum, R.D., Kirk, D.E., 1988, First Principles of Discrete Systems and Digital Signal Processing, Addison-Wesley Publishing Inc., Reading, MA.

## BIOGRAPHICAL SKETCH

The author was born in Kornet Al Hamra, Lebanon in 1973. After finishing his high school education in Lebanon, he moved to the U.S. to pursue his undergraduate degree in Mechanical Engineering at the University of Kentucky. After graduating in 1995, the author moved to Florida to attend graduate school at the University of Florida. He received an M.S. in Mechanical Engineering in 1998 and remained at U.F. to pursue a Ph.D. After graduation the author plans for a career in industry.

I certify that I have read this study and that in my opinion it conforms to acceptable standards of scholarly presentation and is fully adequate, in scope and quality, as a dissertation for the degree of Doctor of Philosophy

John C. Ziegert
Professor of Mechanical Engineering

I certify that I have read this study and that in my opinion it conforms to acceptable standards of scholarly presentation and is fully adequate in scope and quality, as a dissertation for the degree of Doctor of Philosophy

Jacob Hammer
Professor of Electrical and Computer Engineering

I certify that I have read this study and that in my opinion it conforms to acceptable standards of scholarly presentation and is fully adequate in scope and quality, as a dissertation for the degree of Doctor of Philosophy

John K. Schueller
Associate Professor of Mechanical Engineering

I certify that I have read this study and that in my opinion it conforms to acceptable standards of scholarly presentation and is fully adequate in scope and quality, as a dissertation for the degree of Doctor of Philosophy

Paul Mason
Assistant Professor of Mechanical Engineering

I certify that I have read this study and that in my opinion it conforms to acceptable standards of scholarly presentation and is fully adequate in scope and quality as a dissertation for the degree of Doctor of Philosophy

W G Sawyer

W Gregory Sawyer
Assistant Professor of Mechanical Engineering

This dissertation was submitted to the Graduate Faculty of the College of Engineering and to the Graduate School and was accepted as partial fulfillment of the requirements for the degree of Doctor of Philosophy

December 2001

Pramod P Khargonekar
Dean, College of Engineering

Winfred M Phillips
Dean, Graduate School